A STUDY OF MEMBRANE PROPERTIES ON AIR CONDITIONING PERFORMANCE

by

ELIZABETH J. BOYER

B.S., University of Nebraska-Lincoln, 2011

A THESIS

submitted in partial fulfillment of the requirements for the degree

MASTER OF SCIENCE

Department of Chemical Engineering
College of Engineering

KANSAS STATE UNIVERSITY
Manhattan, Kansas

2013

Approved by:

Major Professor
Mary E. Rezac

Abstract

Energy consumption due to heating, ventilation, and air conditioning amounts to 10-20% of global electrical energy usage. Air conditioning alone uses one trillion kilowatt hours globally. This energy is required for the dehumidification of air in addition to its cooling. New membrane technologies have the potential to decrease air conditioning energy requirements by significant amounts. A membrane acts as a partial heat and mass exchanger in conjunction with a traditional air conditioning system to remove water content and reduce the cooling load. Membranes vary according to their properties and method of mass transport. Liquid membranes have high permeability and selectivity, dense membranes have high selectivity and low permeability, and porous membranes have low selectivity and high permeability. A theoretical model was created to observe how membrane properties affected the potential energy savings of such systems. The most influential properties were flow rate, water permeability and selectivity, membrane area and thickness, and the purge flow temperature. Other properties were determined to be minimally important such as outdoor temperature and humidity. The effect on energy savings in many cases was not a linear relationship but suggested an optimal value beyond which energy savings did not significantly increase. The best simulations showed electrical energy savings of 86-95%.

Table of Contents

List of Figures v
List of Tables viii
Chapter 1 - Introduction 1
Energy Context of Air Conditioning Processes 1
Traditional Direct Exchange 2
Membranes 5
Dense Films and Liquids 5
Porous Membranes 7
Membrane Summary 7
Membrane AC Processes 8
Chapter 2 - Model Simulation 13
Membrane module 13
Equations and assumptions 17
Validation 26
Limitations 30
Chapter 3 - Simulation Results 31
Relative Energy Savings 31
Baseline 32
Effect of Outdoor conditions 34
Effect of Purge conditions 39
Thickness 43
Area 45
Feed Pressure 49
Purge pressure 52
Flow Rates 54
Permeation Coefficient and Selectivity 57
Cost Estimates 64
Results Summary 66

Chapter 4 - Conclusions and Outlook 69
References 72
Appendix A - Matlab Model Code 75

List of Figures

Figure 1: Traditional Direct Exchange AC system diagram 2
Figure 2: Psychometric chart of an example DX AC system 4
Figure 3: Supported liquid membrane diagram. 6
Figure 4: Hybrid DX membrane total heat exchange. 9
Figure 5: Psychrometric chart for the membrane-DX system that is in Figure 4. The Red line represents the membrane process, blue is the evaporator, and green is the condenser. 11
Figure 6: Diagram of a hollow fiber membrane module. Original image obtained from http://www.gewater.com/handbook/ext_treatment/fig9-5.jsp. 13
Figure 7: Example of asymmetric hollow fiber membrane. Blue is the support structure, red is the selective layer; the black line represents the membrane thickness. 14
Figure 8: Differential representation of the model. 17
Figure 9: Mass balance model algorithm. Mass balance loop ends after 500 iterations of adjusting P and Y profiles. 20
Figure 10: Energy balance algorithm. Set within the (k) loop of the mass balance loop. 24
Figure 11: L.Z. Zhang's membrane module. Sheets of membrane are stacked vertically inside the module. Photo taken from Zhang 2012. 28
Figure 12: Comparing outdoor humidity levels to the membrane performance by using a psychrometric chart. Feed temperature is constant at 95°F. All other parameters are at base levels (see Table 5). 35
Figure 13: Relative energy savings of several feed humidity levels at a feed temperature of 95°F. All other parameters are at base levels (see Table 5). 36
Figure 14: Psychrometric chart for feed streams of variable temperature, keeping humidity of feed constant at 85%. All other parameters are at base levels (see Table 5). 37
Figure 15: Relative energy savings of varying feed temperature. All other parameters are at base levels (see Table 5). 38
Figure 16: Effect of purge relative humidity at constant temperature of 75°F. All other parameters are at base levels (see Table 5). 39
Figure 17: Relative energy savings for several purge humidity levels. All other parameters are at base levels (see Table 5). 40

Figure 18: Psychrometric chart of the effect of changing the purge stream temperature. All other parameters are at base levels (see Table 5). 41
Figure 19: Trend of relative energy savings with varying purge temperature. All other parameters are at base levels (see Table 5)..... 42
Figure 20: Psychrometric chart for several membrane thicknesses on the dehumidification of air. All other parameters are at base levels (see Table 5)..... 44
Figure 21: Relative energy savings of varying membrane thickness. All other parameters are at base levels (see Table 5). 45
Figure 22: Psychrometric chart for the separation of water from air for membranes of differing area. All other parameters are at base levels (see Table 5). 47
Figure 23: Relative energy savings with varying membrane area. All other parameters are at base levels (see Table 5). 48
Figure 24: Psychrometric chart showing the effect of changing the feed side total pressure while keeping all other variables constant. Feed pressures below 84cmHg use a fan. The feed pressure of 94cmHg is supplied by a compressor. All other parameters are at base levels (see Table 5)..... 51
Figure 25: Relative energy savings with increasing feed pressure. 52
Figure 26: Psychrometric chart for the effect of purge pressure on membrane separation. All other parameters are at base levels (see Table 5)..... 53
Figure 27: Relative energy savings of changing purge pressure. All other parameters are at base levels (see Table 5). 54
Figure 28: Effect of varying feed and purge flow rates. All other parameters are at base levels (see Table 5)..... 55
Figure 29: Relative energy savings of changing flow rates. All other parameters are at base levels (see Table 5)..... 56
Figure 30: Effect of changing the permeability of water while keeping the permeability of air constant at 600 Barrer. All other parameters are at base levels (see Table 5). 59
Figure 31: Relative energy savings by varying selectivities by changing the water permeability selectivity constant at 100. All other parameters are at base levels (see Table 5). 60

Figure 32: Psychrometric chart of the effect of changing the water permeability and keeping the air permeability constant at 400 Barrer. All other parameters are at base levels (see Table 5). 62
Figure 33: Relative energy savings by varying water permeability, keeping air permeability constant at 400 Barrer. All other parameters are at base levels (see Table 5). 63
Figure 34: Final simulation for which membrane properties were set at values close to optimal values for maximizing energy savings. 68

List of Tables

Table 1: Comparison of three membrane types; the dark red represents polymer, white is open volume, or pores, green is dense polymer selective layer, blue is liquid layer. 8
Table 2: Comparison of membrane properties and energy savings of some previous studies. 12
Table 3: Model nomenclature and units 15
Table 4: Simulations of Zhang's system by varying feed pressures and selectivities. 29
Table 5: Baseline input values for the simulations. 33
Table 6: Water permeabilities of various polymers reported in units of Barrer (Welding 2013, Metz 2003) 57
Table 7: This table shows a comparison of costs and benefits of several membrane materials. .. 65
Table 8: Input values for a final simulation. 67

Chapter 1 - Introduction

Air conditioning is an air treatment process to both cool and dehumidify air for health and comfort. There are several systems that have been developed to accomplish this. Systems that have recently been developed use membranes. This section outlines the health benefits and energy requirements of air conditioning systems and describes several types of air conditioning processes.

Energy Context of Air Conditioning Processes

For human health and comfort, an indoor environment must be properly balanced between the flow of air, temperature, and humidity. If indoor environmental conditions are not properly maintained, bacterial diseases such as Legionnaire's disease, Pontiac Fever, Humidity Fever, and "Sick House Syndrome" can widely spread along with property damages caused by mold or condensate (Kistler 2002, Kozubal 2011, Johnson 2003). Healthy humidity levels are considered to be between 35-60% while room temperatures may range between 60-80°F (Kozubal 2011). Heating, ventilation, and air conditioning processes (HVAC) have been designed to treat air under many different environments. Air conditioning (AC) systems are used not just for cooling air, but to lower humidity which means that a unit may be in operation even during cold months.

In the world's residential and commercial sectors HVAC systems account for 50% of building energy consumption which amounts to 10-20% of global electrical energy produced annually (Mahmud 2010). However, during hot and humid seasons, this increases to 20-40% (Zhang 2012). Only accounting for air conditioning, global electrical use is estimated at one trillion kilowatt hours, or around $90 billion (Cox 2012). In the United States 10% of all electricity produced is used for air conditioning (Kozubal 2011). For vehicular AC use, it is estimated that 7-10 billion gallons of gasoline is used per year (Cox 2012). According to 2011 data (EIA 2013) this means that vehicular AC systems consume about 6% of gasoline supplied to the United States in a year.

In Taiwan over 30% of Taiwanese power is spent on air conditioning during the summer months (Chiou 2008), while the city of Mumbai in India uses 40% of its electricity on air conditioning (Cox 2012). Countries such as India and China have a greater demand for air

conditioning than what can be provided. In China over 50 million air conditioning units were sold in 2010, which is over ten times the amount sold in the U.S. in the same year, leading to a shortage of available energy, and resulting in energy rationing (Cox 2012). Because of the decrease in viable energy sources despite the growing demand for energy, and because air conditioning systems account for a good percentage of energy use it has become of great interest in the past two decades to improve or create new AC systems with low energy requirements.

Traditional Direct Exchange

The traditional direct expansion (DX) system in Figure 1 is a mechanical air dehumidification system that is used in the majority of air conditioning processes. Its primary advantages include compactness and a reliance only on electrical energy for operation. Other systems such as absorption columns and desiccant wheels require strong heat sources, which complicate operations (Liang 2010).

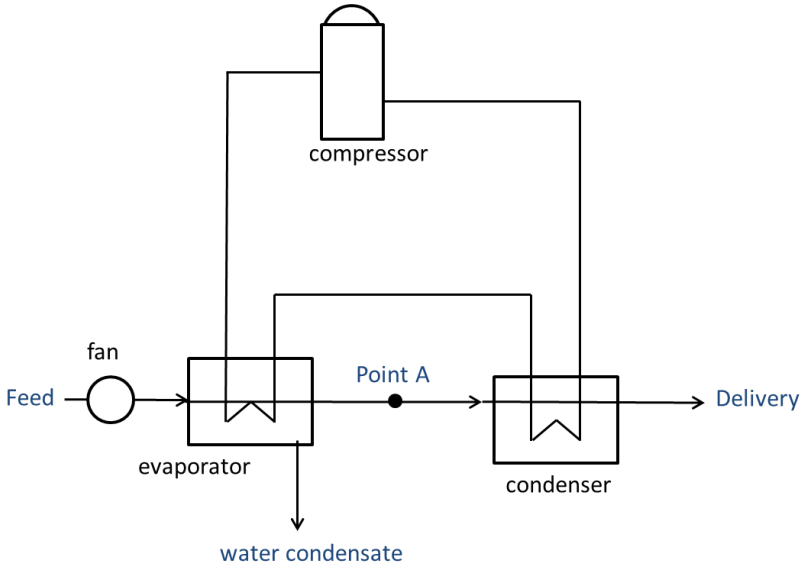

Figure 1: Traditional Direct Exchange AC system diagram

The traditional DX system simultaneously dehumidifies and cools the air by using a compressor, evaporator, and a condenser. A refrigerant liquid is circulated throughout the system while the air is treated by flowing across the evaporator and condenser. Fresh outside air (the feed in Figure 1) is first chilled by the liquid refrigerant and water condenses out of the air based

on its dew point (usually below 45°F at point A in Figure 1). This step of the process occurs in the evaporator, named so because the refrigerant liquid vaporizes from this heat exchange. The refrigerant will then go to the electrically powered compressor where it will be pressured to its saturation pressure producing a liquid. The refrigerant is then sent to a condenser where it exchanges its heat with the saturated air that comes from the evaporator. This will further reduce the temperature of the refrigerant. For the air (from point A to Delivery in Figure 1), the heat exchange from the condenser will heat the air to a temperature more appropriate for indoor conditions.

The refrigerant used in this process was R-22, also called Freon; but it has now been largely phased out because of its disastrous effects on the ozone layer. The most common refrigerants still being used are R-410A and R-134A which are both global warmers with potentials of 2000 and 1300 respectively (Kozubal 2011). Newer refrigeration technologies have allowed environmentally friendly desiccants, which are concentrated salt solutions in water, to replace these harmful refrigerants. The most commonly used salt solution is aqueous lithium chloride (Kozubal 2011).

A psychometric diagram of the air processing by DX is shown in Figure 2 in which the feed air that is hot and humid air is cooled to point A from the evaporator process. The blue curve in the process shows the dehumidification that occurs by condensation as the temperature is lowered. From point A to the delivery point, the air is heated by the condenser which changes its conditions from saturation at 45°F to a humidity of 40% at 70°F.

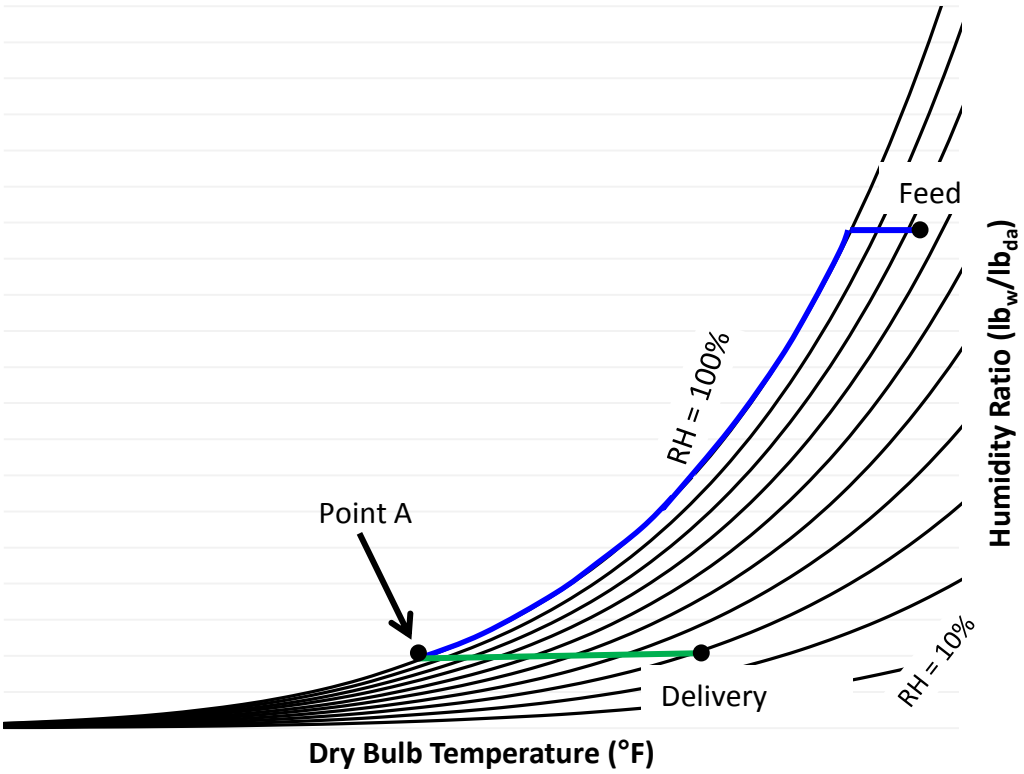

Figure 2: Psychometric chart of an example DX AC system

A DX system consumes more energy for hotter and wetter conditions than it does for colder and drier conditions. This means that the coefficient of performance, or COP, falls dramatically in hot and humid seasons (Liang 2010). For subtropical regions like south and southeast Asia which have an outside humidity between 80-90% for most days of the year (Liang 2010), and because this region is one of the fastest growing in both population and quality of living, the amount of energy used for air conditioning processes will skyrocket. Therefore, it is of great interest to find AC processes that can provide comfortable air at a lower energy cost.

Traditional DX systems have been improved in their energy efficiency by recirculating air, or using exhaust air in partial heat exchange with the outside air. Other energy-saving research has focused on control or mechanical improvements in the fan coils or the compressor. Some studies like these have shown energy savings of 6-13% (Chiou 2008). However, most of these studies only involve mid-to-large sized AC units, while small residential units have not been improved. Furthermore, some indoor air processes must supply 100% fresh outside air such

as hospitals, clean rooms, and laboratories; this requires AC units to operate under extremely high processing loads and will be unable to be improved through recirculation methods.

Membranes

Other improvements to AC units involve research in methods other than DX systems. Some of the most promising of these systems use membranes. A membrane is a material, often polymeric, which acts as a semi-impenetrable barrier. Either due to pores within the membrane or through solution-diffusion, molecules are able to be transported from one side of the membrane to the other. Some membranes are porous which primarily separate molecules based on size. Dense membranes do not have pores; they allow for transport through them by first absorbing the vapor, then the vapor diffuses through the film before desorbing on the other side.

Dense Films and Liquids

Permeation, or the permeability coefficient, is related to the rate of flux of a species through a membrane. The permeation coefficient is dependent on the nature of the membrane material and vapor. If the membrane is a dense film, Permeability is given by:

$$P = S \cdot D$$

P is the permeation coefficient, S is the sorption coefficient, and D is the diffusion coefficient (Baker 2000). This relationship is called the solution diffusion model because it assumes that the membrane polymer matrix is non-porous, and the gas molecules are transported through the film by two mechanisms: sorption and diffusion. Sorption describes the first step in gas transport in which the gas molecule reaches the surface of a dense film and sorbs into the matrix of the membrane. Sorption, or solubility, is a thermodynamic term depending on molecular interactions between the polymer and the penetrant (Costello 1994) as well as condensability and the free volume within the polymer (Wind 2002). Membranes with a high degree of open surface volume will have a higher sorption coefficient than very densely packed membranes.

The second step of dense film gas transport is called diffusion. The diffusion coefficient is an expression of the mobility of the gas through the dense polymer film. It is described by the gaseous molecule "jumping" from one void in the polymer matrix to the next. The distance between two voids is limited by the motion of the polymer chains. The diffusion coefficient is a

function of this distance, as well as the frequency of the "jumps" (Wind, 2002). Diffusion is highly dependent on the mobility of the polymer segments and the packing between them (Koros 2001). Gases have a high diffusion coefficient in liquids and in materials with high free volume (Baker 2000).

Liquids also can be a type of dense membrane, since their thermodynamic behavior of sorption is exactly the same as for dense films, and since diffusion also occurs. However, liquids require mechanical support to contain their shape and prevent them from flowing. Supported liquid membranes are liquids suspended inside of or between solid polymer layers. A diagram of a supported liquid membrane is shown in Figure 3. Since this type of membrane is made from more than one material, it is classified as a type of composite membrane.

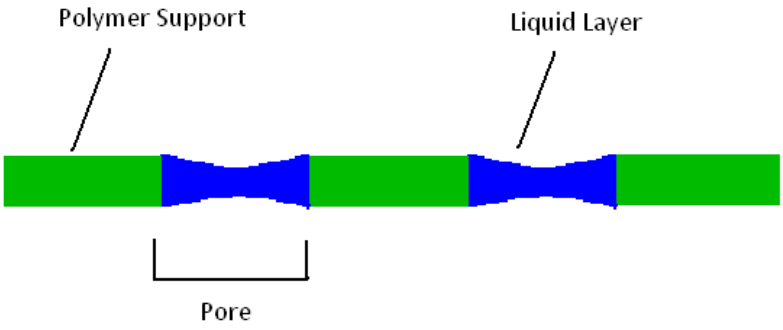

Figure 3: Supported liquid membrane diagram.

The solid polymer support shown in Figure 3 has pores which are filled by the liquid which is held in place by capillary action (Baker 2000). Because of this, the stability of supported liquid membranes is of concern; thicker membranes are generally more stable and so liquid membranes are limited by a minimal thickness.

The vapor molecules will more readily pass through the liquid layer than the polymeric layer because of a higher solubility coefficient, thus flow through the polymeric material is generally neglected, and the permeability coefficient of liquid membranes describes the solubility and diffusivity of vapor molecules in and through the liquid layer. The selectivity of the liquid layer is generally higher than in dense films because of this difference in solubility (Zhang Xiao 2008).

Another type of composite membrane is called an asymmetric membrane. Because solid polymers are more stable than suspended liquids, they are not necessarily limited by small

thicknesses (Baker 2000); however, mechanical integrity may be compromised. A solution for this problem was found by using a support structure underneath the thin dense layer. In order to neglect the impact of the support layer on resistance to mass transfer, the support layer is designed to be porous. In this way, the permeation coefficient is dependent on the thin dense layer and not on the support layer. More information about porous membranes is discussed below.

Porous Membranes

Porous polymers also allow for the transport of gases; however, the mechanism is different from the solution-diffusion method discussed above. Different transport mechanisms in porous polymers may include Knudsen diffusion or Poiseuille flow; both of these are associated with the size of the pores relative to the size of the gas molecules and have different mathematical representations (Baker 2000). These mathematical relationships will not be discussed here.

Porous polymers may have a higher flux of gas molecules than dense or liquid membranes depending on the size of pores (Baker 2000). However, porous polymers have a lower selectivity towards gas transport due to the separation mechanism being physical rather than chemical in nature.

Because the transport behavior of gases varies between hundreds of different polymers, there are a myriad of possible membranes that can be chosen for a given system. Porous membranes generally have a higher permeability, but a low selectivity, while dense films have a high selectivity and a lower permeability. Liquid membranes have still higher selectivity, and a high permeability.

Membrane Summary

A summary of these three types of membranes are shown in Table 1 for which red color represents polymeric material, and white is open volume representing pores. The green layer of the asymmetric membrane is the dense selective layer with no pores on top of a porous support layer. Notice that the dense layer is thinner than the support layer, though the scale in the table is not representative of realistic ratios. The blue color in Table 1 represents the liquid layer suspended inside the pores of a supported liquid membrane.

Table 1: Comparison of three membrane types; the dark red represents polymer, white is open volume, or pores, green is dense polymer selective layer, blue is liquid layer.

Type	Diagram	Flux	Selectivity	Thickness
Porous	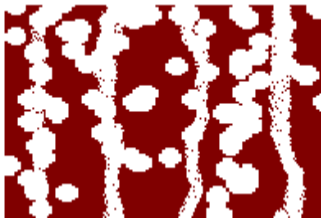	High	Low (1-50) (Metz 2003)	Moderate (higher than 10µm) (Baker 2000)
Dense/solid (asymmetric)	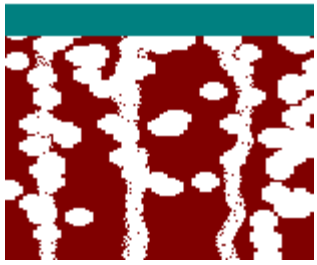	Low	High (50-5,000,000) (Metz 2003)	Small (less than 1µm) (Baker 2000)
Liquid (supported liquid membrane)	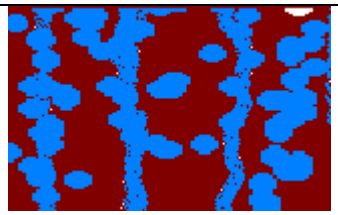	Moderate-High	High ($1x10^5$-$11x10^6$) (Zhang Xiao 2008)	Large (over 100µm) (Zhang Xiao 2008)

Table 1 shows the differences in design of three types of membranes that were discussed as well as displays a comparison of their flux, selectivities, and thicknesses in terms of relative high and low. There are definite advantages and disadvantages to all three types. Because water vapor and air have different permeability coefficients with polymeric materials, separation with a membrane could be used to dehumidify air.

Membrane AC Processes

In a study by Kistler and Cussler (Kistler 2002) poly-ether-sulfone membranes were found to recover 70% of the specific heat and 60% of the latent heat in air processing. This study showed that a membrane system can remove water from an air stream without requiring condensation or the energy associated to do so. In this way, membrane systems reduce the amount of energy required to remove water from air. Kistler and Cussler designed their

membrane system for dehumidification only. To cool the air, the membrane system could be designed to have different temperatures of vapor streams on either side of the membrane; that is to say, a non-isothermal membrane system would have heat exchange.

Another way to cool air that has been dehumidified by a membrane system is to take the retentate stream from the membrane system and feed it into a traditional DX system. This is so that water can be partially removed from the air stream by the membrane part of the system; the air stream is then cooled to appropriate conditions by the DX system. After moisture is removed by the membrane system, the DX system would have a significantly reduced load and could lower the temperature to the desired point at less energy cost. This type of AC system is called a hybrid DX total heat exchanger or membrane-based total heat recovery and is shown in Figure 4. This system utilizes air from indoors as a purge stream in the membrane to transfer heat and moisture with outside air (Nasif 2010, Liang 2010, and Zhang 2012).

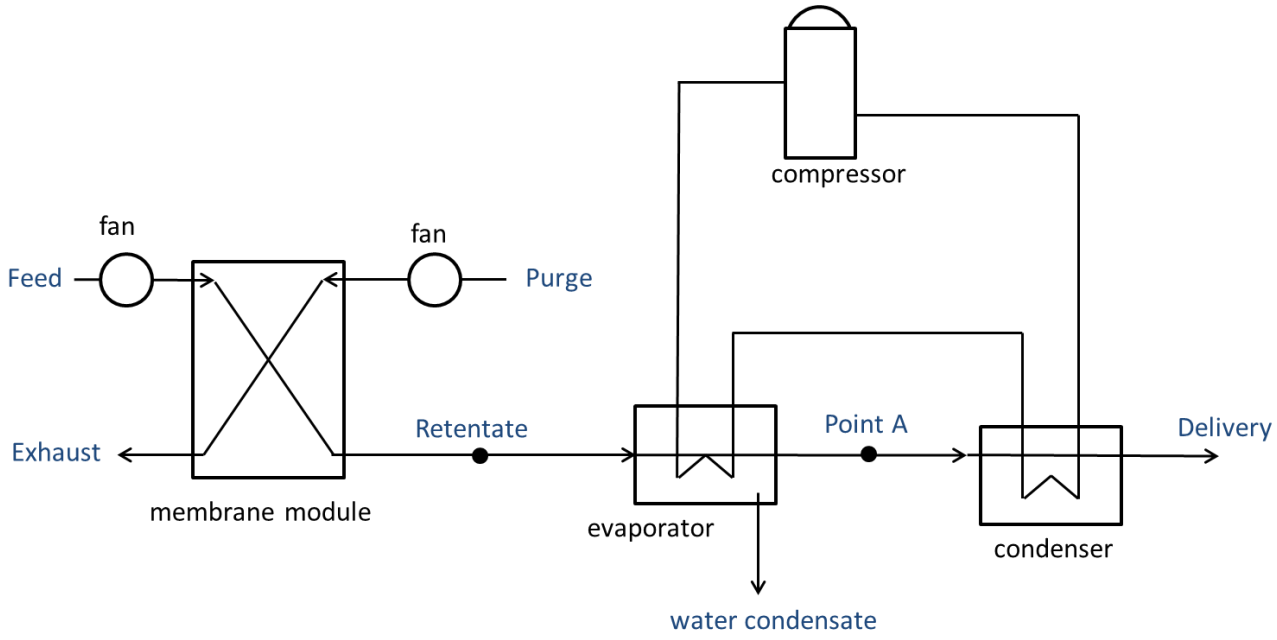

Figure 4: Hybrid DX membrane total heat exchange.

In a study by Nasif et al. using a Kraft paper membrane 8% energy savings in a humid climate with 100% truly fresh air was possible (Nasif 2010). This membrane has micro-pores and separates water vapor from air based primarily on size. Liang and Zhang's studies used a composite membrane of cellulose acetate and polyvinylidene fluoride with LiCl solution, which is a supported liquid membrane acting with solution-diffusion type separation (Liang 2010, and

Zhang 2012). Their estimates showed that their hybrid membrane-DX system could reduce energy use by 70-80%.

The psychrometric chart for this hybrid system is shown in Figure 5. The feed conditions are at a point on the chart that show it is hot and humid. The membrane lowers the humidity ratio though mass transfer of water out of the feed along with some amount of cooling due to heat transfer with the purge stream. This step in the treatment is shown by the red curve in the graph. The point labeled as the retentate has a lower humidity and temperature than the feed; however, the retentate may not have conditions for appropriate indoor comfort levels. Thus, the retentate is sent to the DX portion of the system. The evaporator cools the retentate to saturation and then condenses water out until the desired humidity ratio is obtained. This is shown by the blue curve in Figure 5. At point A, exiting the evaporator, the temperature is too cold (usually around 45°F) for indoor delivery. The air stream is heated by the condenser from point A to the delivery air conditions shown by the green curve in the figure.

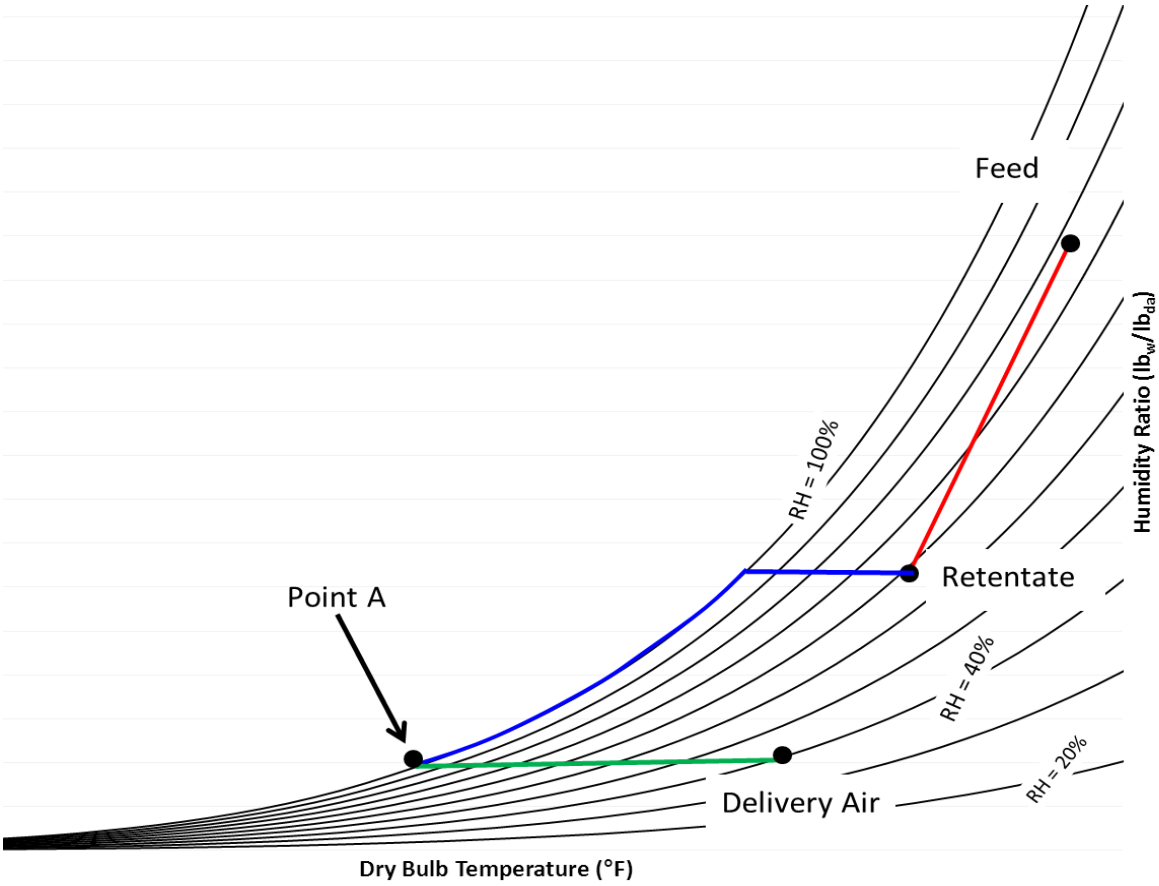

Figure 5: Psychrometric chart for the membrane-DX system that is in Figure 4. The Red line represents the membrane process, blue is the evaporator, and green is the condenser.

The hybrid system shown in Figure 5 lowers energy costs because the retentate conditions contain less water and has a lower temperature than the feed. This reduces the cooling load due to latent and specific heating and cooling required of the electrically powered DX part of the system. It is expected that membrane systems which have a colder retentate with a lower humidity ratio will have higher energy savings than a system which has higher temperatures and water content.

To better compare the membrane AC studies previously conducted on membrane hybrid-DX systems by Nasif et al. and L.Z. Zhang, Table 2 compares their systems' membrane properties to the predicted energy savings. The term NTUm refers to the number of mass transfer units of water that permeate through the membrane, and is related to the membrane's permeation coefficient for water.

Table 2: Comparison of membrane properties and energy savings of some previous studies.

Study	Membrane	Thickness (μm)	Area (m2)	NTUm	Energy Savings[1]
Nasif 2010	Kraft paper, porous	98	n/a	n/a	8%
Zhang 2012	liquid composite PVDF, cellulose acetate, LiCl	142	8	4.2	70-80%

It is difficult to compare the results from the studies shown in Table 2. Neither study has used the same membrane, or membrane properties, for experimental or simulated work, nor have some important membrane properties been recorded in publications. Nasif et al. used a porous membrane, while Zhang used a supported liquid membrane, both of which have different permeability coefficients due to different separation mechanisms as discussed in the previous section. The energy savings shown have a large range from 8-80% according to these studies. It is likely that this large range in energy savings is due to the differences in membranes used in these studies.

Since membrane properties have an effect on the energy and mass flux of a system the optimization of the membrane system would significantly influence overall system efficiency. The previous works discussed above focused on the design of the hybrid systems, while treating the membranes as black boxes. That is to say, these previous works did not focus their research on the membrane part of the hybrid system, but rather on the system as a whole. This present work will focus on the impact of the membrane properties. The purpose of the present study is to determine how important the choice of membrane is in air conditioning systems. This analysis will involve a theoretical model to investigate the behavioral trends of a hybrid membrane-DX system caused by varying membrane properties for a dense membrane.

[1] Energy savings refer to the difference in the amount of energy required by the new system and the conventional DX system, divided by the energy required by the conventional DX system.

Chapter 2 - Model Simulation

To investigate the critical parameters of membrane hybrid-DX systems on energy savings, a simulation was created. The model is based on the hybrid membrane-DX system described in Chapter 1. Chapter 2 describes the model's basic algorithm and equations as well as its limitations and assumptions.

Membrane module

The type of membrane module used in simulations is shown in Figure 6 which has countercurrent flow utilizing hollow fibers. Feed flows inside the fibers and comes out as the treated retentate. The purge flows around the outside of the fibers and strips water away as an exhaust stream.

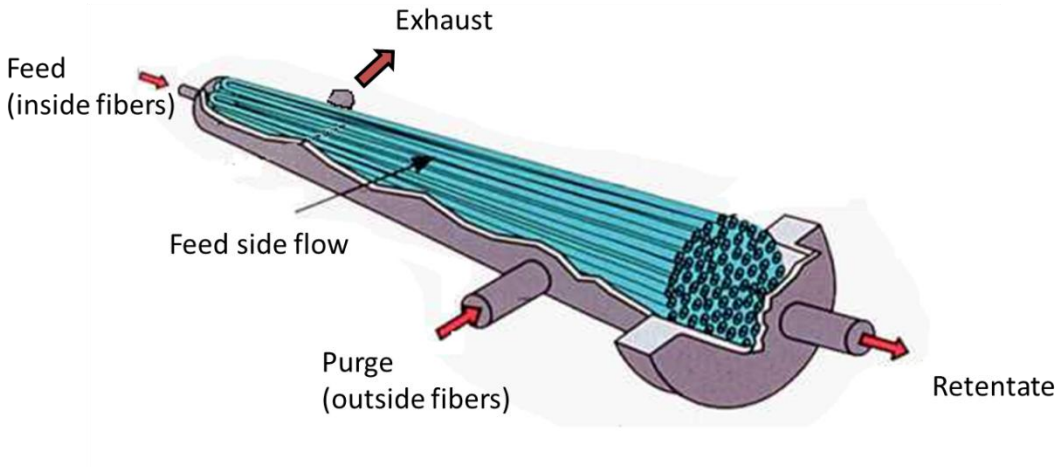

Figure 6: Diagram of a hollow fiber membrane module. Original image obtained from http://www.gewater.com/handbook/ext_treatment/fig9-5.jsp.

A hollow fiber module is made up of rolls of individual polymer cylinders, which are hollow. Each polymer cylinder, or fiber, is long with a comparatively small radius. The membrane thickness is related to the polymer material which causes significant resistance to mass transport; in other words, the thickness of the material that has the lowest permeability coefficient. For a dense film, in which the entire polymer acts with equal resistance, the hollow fiber membrane thickness is simply the difference between the fiber's inner and outer radii. For

asymmetric membranes, the selective or resistive layer is made up of one polymer while the rest of the membrane is made up of a comparatively non-resistant support layer for mechanical stability. This is shown in Figure 7 where the red section represents the selective layer; the black line is the thickness of that layer; the blue section represents a support layer. The support layer is required because very thin materials are likely to break from any small disturbance. Furthermore, during the membrane casting process, thin membranes are more likely to develop faults and weaknesses. The support layer provides a stable material with which the selective layer may adhere to. In these asymmetric membranes the membrane thickness refers to the thickness of the selective layer only.

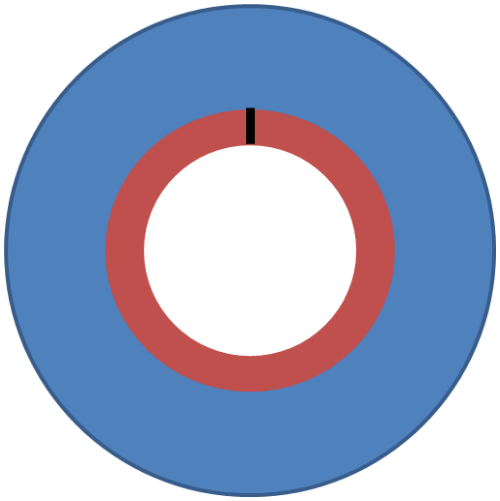

Figure 7: Example of asymmetric hollow fiber membrane. Blue is the support structure, red is the selective layer; the black line represents the membrane thickness.

Figure 7 shows what an asymmetric membrane would look like in a hollow fiber designed module. However, other designs are possible. A flat plate module is exactly a flat slab of support layer with the thin selective layer spread out on top. Another type of module is called a spiral wound module. This type of module is more complicated than either flat-plates or hollow fibers, though it is made by stacking multiple layers of flat plate membranes and then spirally rolling them up into a tube (Baker 2000). The advantage of using hollow fibers or spiral wound membranes is that the area of the membrane can be maximized without dramatically increasing the size of the module.

The area of the membrane describes the surface area. Regarding the hollow fiber module, for both dense films and asymmetric membranes the area is the surface area which involves the

inner radius of the fibers and their length. The membrane area of the module is a function of each fiber's surface area and the total number of fibers that can be packed into a module.

The area and thickness are two properties that are required to model the flux of gases through a membrane. Table 3 lists the other variables that were used in the model. Some of the variables are shown with their conventional symbols, while others have been given some other symbol to avoid confusion within the program. The model was created using MATLAB 2011 for which the code is included in Appendix A - .

Table 3: Model nomenclature and units

Input Variable	Unit	Description
A	m^2	Total membrane surface area
a	m^2	Differential membrane surface area
C_{min}	J/s/K	Minimum capacity of heat transfer
COP		Coefficient of Performance
cp	J/kg/K	Constant specific heat capacity of air at 300K
Cr		Capacity ratio
Da	Barrer	Permeability of water
Db	Barrer	Permeability of the air
Diam	m	Inner diameter of the membrane fibers
E	mol/s	Exhaust flow rate
ee or ε		Effectiveness
F	mol/s	Feed flow rate
H	J/mol	Enthalpy
hc	W/m^2/K	Heat transfer coefficient of air on the membrane cold side
hh	W/m^2/K	Heat transfer coefficient of air on the membrane hot side
h_{mem}	W/m^2/K	Heat transfer coefficient of the membrane
H_{vap}	J/mol	Heat of vaporization of water
i		The position along the membrane
kair	W/m/K	Constant thermal conductivity of air at 300K
L	m	Length of the membrane
mwat	kg/s	Mass flow rate of water in feed

n		Number of discrete positions along the membrane
NTU		Number of transfer units (heat exchange)
NTUm		Number of mass transfer units
Nuc		Nusselt number on the cold side of the membrane
Nuh		Nusselt number on the hot side of the membrane
P	mol/s	Purge flow rate
pf	cmHg	Total pressure of the feed
pp	cmHg	Total pressure of the purge
Pr		Constant Prandtl number at 300K for air
q	J/s	Heat transfer rate
$Q._{cond}$	W	Energy required by the condenser
Q_{DX}	W	Energy required by the DX system
Q_{evap}	W	Energy required by the evaporator
q_{max}	J/s	Maximum heat transfer rate
Q_{mem}	W	Energy required to treat air in the membrane
R	mol/s	Retentate flow rate
Relc		Reynolds number on the cold side of the membrane
Relh		Reynolds number on the hot side of the membrane
t	m	Membrane thickness
Tc	K	Temperature on the cold side of the membrane
Tco	K	Temperature on the cold side leaving the discretized membrane fiber
Tf	K	Temperature of the feed air
Th	K	Temperature on the hot side of the membrane
Tho	K	Temperature on the hot side leaving the discretized membrane fiber
Tp	K	Temperature of the purge air
U	W/m^2/K	Overall heat transfer coefficient in the membrane
visc	m^2/s	Constant viscosity of air at 300K
W	mol/s	Total flow through the membrane
wa	mol/s	Water flow through the membrane

W_{comp}	W	Electrical work of the compressor
W_{DX}	W	Work of a traditional DX system
W_{fan}	W	Work of a fan
x		Mole fraction of water on feed side
y		Mole fraction of water on purge side
Y		Guess values for the mole fraction of water on purge side

Equations and assumptions

Most of the equations listed in this section are mass and heat balances. Mass balance equations are based on gas flux equations described in Baker's *Membrane Technology and Applications* (Baker 2000). Heat and energy balances come from Incropera et al. *Fundementals of Heat and Mass Transfer* (Incropera 2007).

To solve mass transport, an algorithm was set up using simple mass balances and membrane flux calculations. To achieve this, the model divided the membrane into "n" number of differential pieces of equal lengths as shown in Figure 8. Calculations were performed in a step-by-step iteration as described in more detail below. Each step is denoted with the symbol "i" which has values between one and "n". The flow rates and composition variables are also represented in Figure 8.

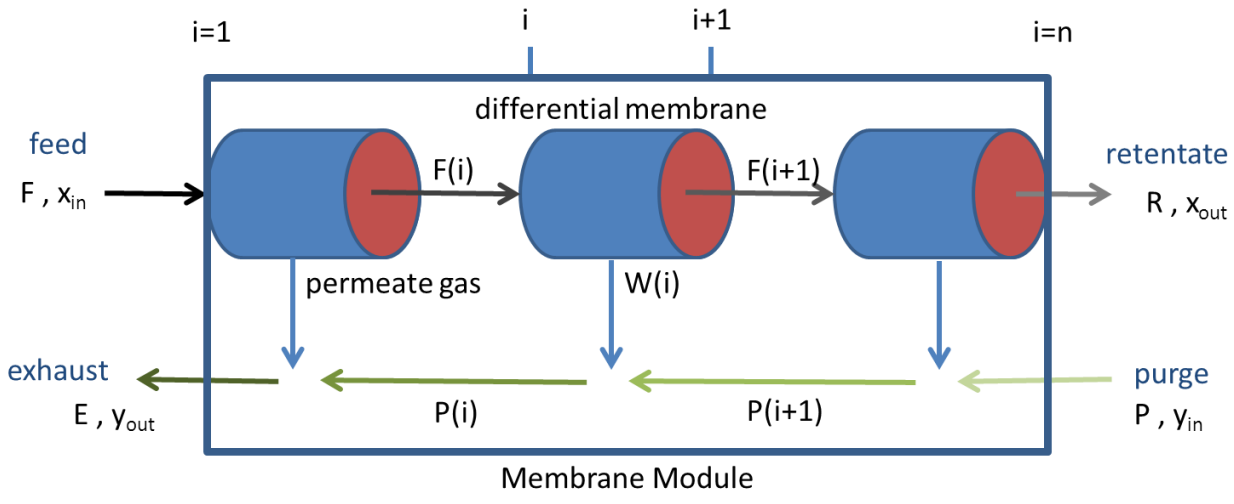

Figure 8: Differential representation of the model.

Equation 1 shows how the composition of water at the "i"th step on the purge side of the membrane may be calculated from terms that describe the amount of water permeating into the purge side plus the amount of water already on the purge side divided by the total amount of water and air flowing on the purge side. The terms that are multiplied by D_a or D_b describe the flux of water and air respectively passing through the membrane and into the purge stream. Although Equation 1 involves Y(i), which is a guessed variable, the iterative nature of the algorithm will eventually converge to calculated composition values, called y(i), that have no dependence on the initial guess values of Y(i). The algorithmic method is shown in Figure 9.

$$y(i) = \frac{\left[\frac{D_a}{t}\cdot(pf\cdot x(i) - pp\cdot Y(i))\right] + P(i)\cdot Y(i)}{\left[\frac{D_a}{t}\cdot(pf\cdot x(i) - pp\cdot Y(i))\right] + P(i) + \left[\frac{D_b}{t}\cdot[pf\cdot(1 - x(i)) - pp\cdot(1 - Y(i))]\right]} \quad (1)$$

Equation 2 describes the flow of water passing through the membrane at the ith step and it depends upon the discretized area "a", the permeability of water "D_a", the partial pressure of water on the feed side "pf*x(i)", and the partial pressure of water on the purge side "pp*y(i)".

$$wa(i) = a\cdot\frac{D_a}{t}\cdot(pf\cdot x(i) - pp\cdot y(i)) \quad (2)$$

Equation 3 calculates the total flowof both water and air through the membrane.

$$W(i) = wa(i) + a\cdot\frac{D_b}{t}\cdot[pf\cdot(1 - x(i)) - pp\cdot(1 - y(i))] \quad (3)$$

Equation 4 calculates the new composition of water at the next "i" step along the membrane. This equation also marks the last calculation needed at a single position before the step moves forward and calculations will begin again at a new position with Equation 1.

$$x(i + 1) = \frac{x(i)\cdot F(i) - wa(i)}{R(i)} \quad (4)$$

Equation 5 adjusts the purge flow rate by adding the amount of water and air that have passed through the membrane to the purge flow. Since the purge flow is countercurrent to the flow of the feed and the (i) direction, Equation 5 calculates in a backwards direction as shown by "n-i".

$$P(n-i) = P(n-1-i) + W(n-1-i) \tag{5}$$

Equation 6 also steps backwards and adjusts the purge side guess compositions based on the calculated water flux and the adjusted purge flow rates

$$Y(n-i) = \frac{y(n-1-i)\cdot P(n-1-i) + wa(n-i)}{P(n-i)} \tag{6}$$

Equation 5 and Equation 6 mark the end of one (k) loop. With the adjustment of P(i) and Y(i) to better guess values the (i) loop is again performed with Equation 1 back to the starting (i) location in the membrane. It was determined that that the initial guesses for E and Y did not have any impact on the final calculated values of P(i) and Y(i), and also that the results reach convergence at over 400 iterations of the (k) loop. Figure 9 shows the algorithm used to solve the mass transport model.

Several key assumptions for mass transport include:

- Feed and purge total pressures are constant.
- Only two substances are present, water and air. Air is treated as a combination of 79wt% nitrogen and 21wt% oxygen.
- Transport through the membrane is only due to absorption and diffusion, not convection.
- Mass transport acts like flow through a flat plate rather than considering flow inside or across a tube.
- Temperature has no effect on the permeabilities of air and water. This seems to be a reasonable assumption since the temperature range in the membrane system is small (Kistler 2002).

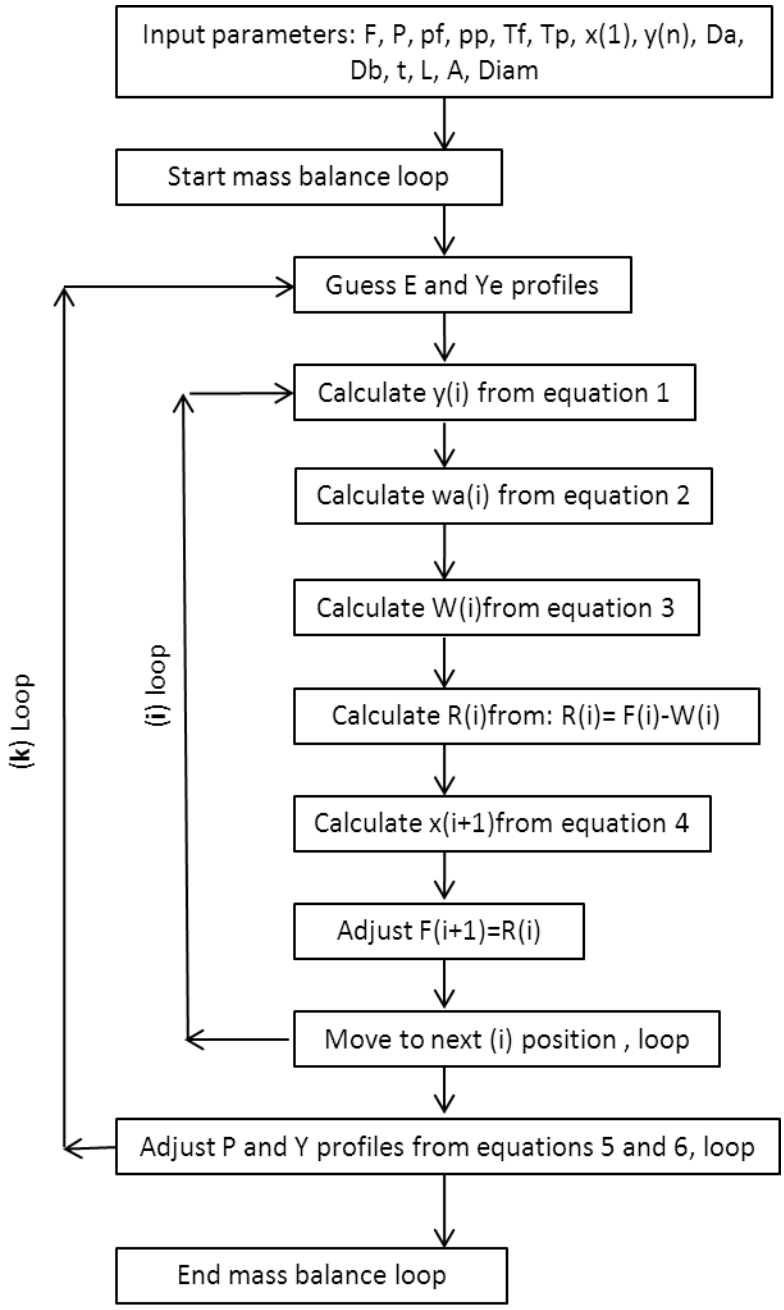

Figure 9: Mass balance model algorithm. Mass balance loop ends after 500 iterations of adjusting P and Y profiles.

For the heat transfer model, both the NTU and simple energy balance methods were used in conjunction; Figure 10 shows the algorithm. It begins by guessing the exhaust temperature and guessing a temperature profile for the purge side of the membrane. Once again, the iterative

nature of the model eventually converges such that the initial guessed temperature profiles will have no impact on the final calculated results.

Equation 7 shows how the Reynolds number was calculated for tubular flow of both the feed and purge sides.

$$Relh = \frac{F(i)\cdot 4\cdot L}{visc\cdot Diam^2\cdot \pi} \quad \text{and} \quad Relc = \frac{P(i)\cdot 4\cdot L}{visc\cdot Diam^2\cdot \pi} \tag{7}$$

Equation 8 calculates the Nusselt number for turbulent flows for which the Reynolds number is greater than 5000. For either the hot or cold side, the Reynolds number "Rel" will be either the hot side Reynolds number "Relh" or the cold side Reynolds number "Relc". Equation 9 calculates the Nusselt number for laminar flows where the Reynolds number is equal to or less than 5000. Both Equations 8 and 9 are correlated relations according to Incropera et al..

$$Nu = 0.0296 Rel^{\frac{4}{5}} \cdot Pr^{\frac{1}{3}} \tag{8}$$

$$Nu = 0.664 Rel^{\frac{1}{2}} \cdot Pr^{\frac{1}{3}} \tag{9}$$

The heat transfer coefficients are calculated from Equation 10 which may be for either the hot (hh) or cold side (hc) flows. The overall heat transfer coefficient is calculated from Equation 11, for which Kistler and Cussler have stated that contributions from the heat transfer coefficient of the membrane, $1/h_{mem,}$ is negligible compared to either of the other heat transfer coefficients and may be dropped out of the equation.

$$h = Nu\cdot \frac{k_{air}}{L} \tag{10}$$

$$\frac{1}{U} = \frac{1}{h_h} + \frac{1}{h_c} + \frac{1}{h_{mem}} \tag{11}$$

For the NTU method the minimum capacity is calculated by Equation 12, whichever version of the equation gives the smallest value will be C_{min}, while the greater value is C_{max}. The capacity ratio is calculated by Equation 13.

$$C_{min}(i) = cp_h \cdot m_h(i) \quad \text{or} \quad C_{min}(i) = cp_c \cdot m_c(i) \tag{12}$$

$$Cr(i) = \frac{C_{.min}(i)}{C_{.max}(i)} \tag{13}$$

The value of the heat NTU is given by Equation 14.

$$NTU(i) = \frac{U \cdot a}{C_{min}(i)} \tag{14}$$

The value of q_{max}, which is the maximum possible heat transfer rate, is calculated from Equation 15.

$$q_{max}(i) = C_{min}(i) \cdot \left(Th_{in}(i) - Tc_{in}(i)\right) \tag{15}$$

The effectiveness is given by Equation 16 which is a correlation from Incropera et al. for countercurrent flow in a concentric tube with Cr(i) <1. This is the only equation in the model which differentiates between a hollow fiber module design and a flat plate module design. To model a module different from hollow fiber, this equation would have to be adjusted.

$$\varepsilon(i) = \frac{1 - e^{-NTU(i)\cdot(1-Cr(i))}}{1 - Cr \cdot e^{-NTU(i)\cdot(1-Cr(i))}} \tag{16}$$

The actual heat transfer rate is given by Equation 17.

$$q(i) = \varepsilon(i) \cdot q_{max} \tag{17}$$

The hot side temperature profile can now be calculated by Equation 18.

$$T_h(i+1) = T_h(i) - \frac{q(i)}{F(i) \cdot cp_h \cdot [18 \cdot x(i) + 26 \cdot (1 - x(i))]} \tag{18}$$

The cold side may now be adjusted and guess values updated to better match with calculations. This is done by stepping backwards in position through the membrane and re-evaluating the cold side temperature profile in Equation 19

$$T_c(n-i) = T_c(n+1-i) + \frac{q(n+1-i)}{P(n+1-i) \cdot cp_h \cdot [18 \cdot y(n+1-i) + 26 \cdot (1 - y(n+1-i))]} \tag{19}$$

With the new cold side profile, the calculations will loop back to Equation 7. Convergence is reached by checking the hot side profile such that it matches the energy balance given by Equation 20.

$$T_h(i+1) = T_h(i) - \frac{P(i)}{F(i)} \cdot \left(T_c(i) - T_c(i+1) \right) \tag{20}$$

The important assumptions in this energy solution include:

- Properties of air (cp, kair, and visc) are constant.
- Assume no heat change caused by water condensation within the membrane.
- Energy is exchanged only by external convection; boundary layer transport was neglected because heat transfer through the membrane was directly related to mass transfer.
- Conduction and radiation was neglected because the membrane was stated to have negligible heat conductivity (k_{mem} was eliminated) (Kistler 2002).

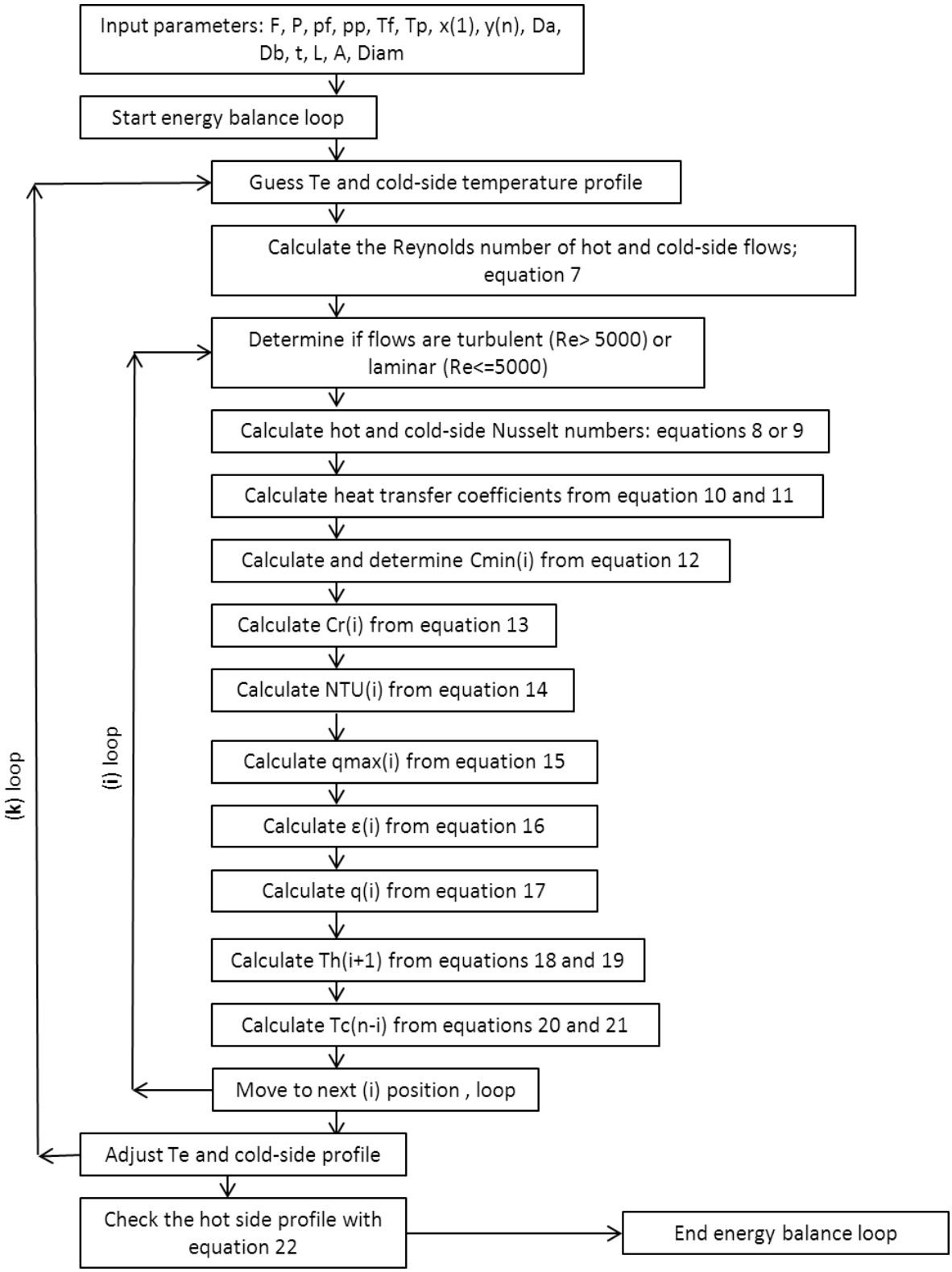

Figure 10: Energy balance algorithm. Set within the (k) loop of the mass balance loop.

After the heat and mass transport solutions were found, the energy savings were determined by comparing the performance of a membrane system retrofitted with a DX system, shown in Figure 4, to a DX system with no membrane, shown in Figure 1. A psychrometric representation of Figure 4 is shown in Figure 5. The feed stream designates the air entering the membrane, while the retentate is the treated air leaving the membrane. The air stream point labeled "Point A" in Figure 5 and Figure 4 describes the saturated air at a cold temperature that comes out of the evaporator. The delivery air is at the desired air conditions for delivery into an indoor room.

For energy analysis, the enthalpy change between the feed and retentate is related to the energy flow of the membrane, called Q_{mem} and given by Equation 21 which is also equal to the work the membrane does to the air.

$$Q_{mem} = F(n)\cdot H(n) - F(1)\cdot H(1) \tag{21}$$

W_{DX} is the work required by the evaporator and condenser in a traditional DX system to affect the enthalpy changes associated with the process of cooling the air exiting the membrane, condensing the water to reach the desired relative humidity, and heating to reach the desired temperature. The mathematical representations of these energy processes are given in Equations 22, 23, and 24. The enthalpies involved in these calculations were obtained by using a downloadable program called kw Psychrometric Functions for Microsoft Excel.

$$Q_{evap} = \left(H_A \cdot F(n) - H_{retentate} \cdot F(n) \cdot \frac{x_{delivery}}{x(n)} \right) + H_{vap} \cdot \left(F(n) - F(n) \cdot \frac{x_{delivery}}{x(n)} \right) \tag{22}$$

$$Q_{cond} = H_{Delivery} \cdot F(n) \cdot \frac{x_{delivery}}{x(n)} - H_A \cdot F(n) \tag{23}$$

$$W_{DX} = Q_{evap} + Q_{cond} \tag{24}$$

W_{comp} is the electrical work required by the compressor to regenerate the refrigerant, which must be related to the work done by the condenser and the evaporator as shown in Equation 25. Since the evaporator heats up the refrigerant and the condenser cools the refrigerant, the compressor must regenerate the energy between these two processes. The enthalpy changes of the refrigerant are opposite and proportional to the enthalpy change of the air. The efficiencies of the evaporator and condenser in Equation 25 were set at 90% and describe a non-insulated heat transfer process for which energy is lost to the surroundings. For a perfectly insulated DX system, these efficiencies would be 100%.

$$W_{comp} = \frac{\frac{Q_{evap}}{efficiency_{evap}} - \frac{Q_{cond}}{efficiency_{cond}}}{efficiency_{comp}} \quad (25)$$

The work of the fans to provide flow and pressure in the membrane was given by Liang (Liang 2010) shown in Equation 26. The numbers represent conversion units such that the work of the fan is in Watts. A fan can provide pressures within 8cmHg within atmospheric pressure and has efficiencies on the order of 60-85% depending on the size and type (Bureau 2013).

$$W_{fan} = F \cdot \frac{(pf - 76) \cdot 224141333}{100^3 \cdot 3600\, efficiency_{fan}} \quad (26)$$

The COP was calculated using Liang' definition shown in Equation 27 (Liang 2010).

$$COP = \frac{Q_{mem} + Q_{DX}}{W_{fan} + W_{comp}} \quad (27)$$

Energy savings are described by comparing the energy use of the membrane-DX hybrid system to energy use for a conventional DX system. The energy calculations of a conventional DX system have the same equations as above, except that there is no retentate stream. The energy savings are calculated as shown in Equation 28.

$$Energy_{Savings} = \frac{\left(W_{feed.fan.DX} + W_{comp.DX}\right) - \left(W_{feed.fan} + W_{purge.fan} + W_{comp}\right)}{W_{feed.fan.DX} + W_{comp.DX}} \quad (28)$$

Validation

To validate the model, the system by L.Z. Zhang (Zhang 2012) was utilized by the simulation. This system involves a membrane combined with a DX system similar to that shown in Figure 4. The membrane used by Zhang was a composite membrane of cellulose acetate and polyvinylidene fluoride with aqueous LiCl solution which was shown to reduce energy use by 70-80%. Zhang's data was used for validation because the system is nearly identical with the system used by the current model and because much of the necessary information was reported in Zhang's publications.

Zhang's input conditions were feed air at 35°C and 70% relative humidity with air flow rate of 200 m^3/h; desired delivery conditions were 20°C and 53% humidity; and purge conditions

were 27°C with 53% humidity. The membrane NTUm was 4.2 with an area of $8m^2$. The final COP of these conditions was calculated to be 5.8 from Zhang's system experiments.

Among the membrane community it is common to refer to permeability in units of Barrer. One Barrer equals 10^{-10}*cm^3(STP)*cm/(cm^2*sec*cmHg). These terms describe the volumetric flow rate of vapor passing through the membrane, the area and thickness of the membrane, and the partial pressure difference between the feed and purge sides of the membrane which is the driving force causing transport. The relationship between NTUm and permeability is shown in Equation 29. This equation assumes that transport is not caused by convection. Note that since Zhang used a supported liquid membrane, the NTUm describes the mass transport through the entire composite material, while a true permeability coefficient would actually be a description of the solution-diffusion of the vapor through just the liquid layer. Because of this, the permeability of water shown by D_a in Equation 29 is actually an apparent or relative permeability.

$$NTU_m = 10^{-10} \cdot \frac{A}{m_{wat}} \cdot \frac{D_a \cdot (pf \cdot x - pp \cdot y)}{t} \cdot \frac{1}{22414} \cdot \frac{18}{1000} \cdot \frac{100}{1} \tag{29}$$

For the current simulation, it was necessary to estimate some of the values that were not provided by Zhang. One such variable was the length of the membrane fibers, which was estimated to be between 10 and 100cm long, however the simulation's results were not affected by these values so a length of 20cm was used in further simulations. This appears to be an adequate estimate based on visual examination of Zhang's membrane module, which is shown in Figure 11. Zhang's module is of a flat-plate design which only differs from the current hollow fiber model by Equation 16.

Figure 11: L.Z. Zhang's membrane module. Sheets of membrane are stacked vertically inside the module. Photo taken from Zhang 2012.

The thickness of the membrane was determined to be 142μm as described by Zhang and Xiao in their description of the membranes that were used in Figure 11 (Zhang, Xiao 2008). It is composed of three layers, two polyvinylidene fluoride layers that are 45μm thick and a porous cellulose acetate layer with LiCl solution that is 52μm thick. This membrane is a supported liquid membrane, while the one used in the model are solid membranes. This difference does not directly affect the model, but rather points out differences in membrane property values. Supported liquid membranes can have higher permeabilities and selectivities than a solid membrane, but solid membranes, specifically asymmetric membranes, can be thinner than 1μm.

Neither the selectivity nor the pressure in the membrane was mentioned in Zhang's publications, other than stating the membrane had an "inherent high selectivity". Since porous membranes do not have selectivities higher than 150, this value was used and considered to be an adequate interpretation of Zhang's statement regarding the selectivity. Similarly, the pressure had to be estimated based on logical assumptions regarding the capabilities of fans. The pressure on the purge side was set at 76cmHg, which atmospheric pressure. The feed-side pressure was chosen at 80cmHg because this would provide a reasonable pressure difference with the purge side but would not be so high that a fan would be unable to provide it.

The efficiencies of the compressor, evaporator, and condenser were all assumed to be 90%, which is very good for such equipment. Fan efficiencies were set at 85%, which is a high value for an axial fan (Bureau 2013).

The results of this simulation as compared to Zhang's results are shown in Table 4. The COP error refers to the error that was calculated by comparing Zhang's COP with the COP that the simulation found. The energy savings error refers to the error associated with comparing Zhang's maximum energy savings of 80% to the energy savings calculated by the simulation. The first run using the values of feed pressure and selectivity as was discussed above had a COP error of 27%, but an energy savings correlation effort of 7%. To understand how much impact and range the estimated values gave to the results, further simulations were run with differences in the selectivity and feed pressure shown in Table 4.

Table 4: Simulations of Zhang's system by varying feed pressures and selectivities.

	Run 1	Run 2	Run 3[2]	Run 4	Run 5
Feed pressure (cmHg)	80	84	100	80	80
Selectivity	300	300	300	150	500
COP error	27%	22%	0.4%	27%	27%
Energy Savings error	7%	4%	3%	7%	7%

By examination of Table 4, the current model's correlations with Zhang's results are acceptable, though they range from 0.4-27% based on the values of feed pressure and selectivity which had to be estimated. It appears as though the feed pressure has the most influence in the range of errors observed in both COP and energy savings error. The choice of selectivity appeared to have no effect on error. Error may also be associated with the difference in module design. Zhang's module was of flat-plate design, while the model assumes a hollow fiber arrangement. The only equation affected would be Equation 16, which relates the effectiveness to the NTU of energy transfer. Other sources of error may be in the assumed compressor, evaporator, and condenser efficiency values.

Because these estimations give results within an acceptable margin of error with Zhang's results, the model with the described equations and algorithms is considered validated.

[2] This feed pressure was calculated assuming the use of a compressor. All other results on this table were calculated using fan energy equations at the set pressure. Details about compressor calculations are discussed in Chapter 3: Feed Pressure results.

Limitations

As with almost any calculation or simulation, this model has some limitations. Depending on the membrane properties and flow rates, it is possible for either the retentate or the exhaust air to become saturated with water. The model will issue a note indicating this, but calculations will continue as if condensation does not occur. Heat exchange in the membrane is calculated without regard to heat of condensation. Also, inhibition of membrane performance due to condensation is not considered.

A second limitation with the simulation is that under certain conditions the model might predict that the feed side temperature is cooled below the purge side's minimum temperature. This is a physical impossibility, and so the retentate temperature must be manually adjusted. Furthermore, the equilibrium temperature obtained by air permeating from the feed side and mixing with the purge is not considered.

The energy analysis also always assumes that an evaporator and condenser are used together, and that condensation always occurs in the evaporator. This means that even if the retentate from the membrane has been treated to near desired air conditions, the retentate will still be treated by both the evaporator and condenser and energy usage will reflect that. Therefore, adjustments have to be made to the energy analysis to account for retentate that does not need DX treatment, or for retentate that only needs slight cooling without further dehumidification.

Chapter 3 - Simulation Results

Hybrid membrane DX systems have the potential to decrease energy requirements for air conditioning. These systems have been researched in growing detail for the past 20 years. These previous studies have shown that energy savings of 8-80% are possible, however many of these studies lack details about the behavior of the membrane system and the influence its properties have on the overall energy requirements. In order to investigate the effects of membrane properties on the energy use of a total membrane heat exchanger (system diagram shown in Figure 4), a model was created as described in Chapter 2. After validation of this model with Zhang's (Zhang 2012) results, membrane properties were changed and simulations were run to investigate the effect of membrane system properties on the energy savings. These simulated results are discussed in more detail below.

Relative Energy Savings

Because a membrane's main function is to enable gases to permeate from the feed side to the purge side, the flow rate of the retentate will be less than that of the feed. For a membrane-DX hybrid system, the retentate is then supplied to the DX portion of the system. This means that the air flow rate that ultimately is delivered to the indoor environment is less than the flow rate of the outdoor feed air entering the membrane. This decrease in flow rate is a concept not encountered in the traditional DX system. To fairly compare the hybrid system to the traditional system, energy should be defined not only by energy used but by energy used per unit of treated supply air that is delivered.

Energy savings are defined as the percentage of electrical energy that is required by a traditional DX system, but is not required by a membrane hybrid DX system. In other words, energy savings is the amount of electrical energy that is saved by switching from a traditional system to a hybrid system. Mathematically, this is represented by Equation 30 below.

$$\text{Energy}_{\text{Savings}} = \frac{\left(\text{Energy}_{\text{Traditional.DX}}\right) - \left(\text{Energy}_{\text{Membrane.Hybrid.System}}\right)}{\text{Energy}_{\text{Traditional.DX}}} \tag{30}$$

To better describe the energy savings, a new term, called the relative energy savings, was calculated. The relative energy savings shows the difference between the feed flow and the

delivered air flow (which is essentially the difference in flow rate between the feed and the retentate); this calculation, shown by Equation 31, is the calculated energy savings normalized by the fraction of delivery flow rate.

$$\text{Relative}_{\text{Energy.Savings}} = \text{Energy}_{\text{Savings}} \cdot \frac{\text{Retentate}_{\text{Flowrate}}}{\text{Feed}_{\text{Flowrate}}} \tag{31}$$

In this way, the comparison of energy savings will be a function of the amount of air that is completely treated and supplied to an indoor environment.

The energy savings calculated in Equations 30 and 31 compare the hybrid system to a simple traditional DX system, which is shown in Figure 1. Note that more modern DX systems have been altered from the simplistic traditional DX system. The modern DX systems may involve a secondary condenser, expansion valves, or air recycling and mixing. Different energy savings would exist if one were to compare a hybrid system to a non-simple, modern DX system.

Baseline

The standard model conditions were based on the design and operation recommendations of a PDMS membrane module obtained from MedArray Incorporated. This module was chosen because PDMS is a commonly used polymeric material and has membrane properties appropriate for the removal of water from an air stream. The MedArray module has a suggested maximum flow rate of 0.002 mol/sec of air for an area of 2500cm^2. Rather than using a theoretical membrane module, the MedArray module provides realistic membrane system properties. For a theoretical module, any flow rate could be paired with any membrane area or thickness, this would be misleading because an extremely high flow rate may have significant pressure drop within the module; while a low flow rate with a thin membrane and large area may have no retentate—the feed would all permeate through the membrane and no flow would be left to form the retentate. For these reasons, the MedArray module was selected to guide the choices for simulating membrane properties. Note that the dense PDMS membrane used in this model has a permeability that is significantly lower than the liquid membrane used by Zhang (Zhang 2012), but larger than the porous membrane used by Nasif et al. (Nasif 2010).

For the simulated air conditions, desired delivery air was set at 68°F and 40% relative humidity. Outside air conditions were set at 95°F and 85% humidity; while the purge air was set

at 75°F and 60% humidity. Atmospheric pressure was assumed constant at 76cmHg. The input variables at their standard values are shown in Table 5. Unless otherwise stated, the values of these variables are not changed.

Table 5: Baseline input values for the simulations.

Inputs	Value
Tf (°F)	95
Tp (°F)	75
pf (cmHg)	80
pp (cmHg)	76
Da (Barrer)	36000
Db (Barrer)	347
t (cm)	0.0055
F (mol/s)	0.002
P (mol/s)	0.002
L (cm)	8.26
A (cm^2)	2500
x(1)	0.043897
y(n)	0.016

The DX compressor, evaporator, and condenser efficiencies were assumed to be 90%. To provide the desired air pressure on the feed and purge sides either a fan was used or, for pressures above 84cmHG or below 70cmHg, an air compressor was used. Both the fans and air compressor efficiencies were assumed to be 85%. These efficiencies value were not changed throughout all of the following results.

A method to estimate quality for simulations has not previously been established in the membrane-AC community. However, for this study, a quality metric was defined to be related to the efficiency of enthalpy exchange between the feed side and the purge side of the membrane as shown in Equation 32. This assumes no heat loss to the surroundings, such that perfect heat exchange inside the membrane would have a quality metric of 100%.

$$\%\text{Quality} = \frac{\left(\text{Enthalpy}_{\text{Exhuast}} - \text{Enthalpy}_{\text{Purge}}\right)}{\text{Enthalpy}_{\text{Feed}} - \text{Enthalpy}_{\text{Retentate}}} \tag{32}$$

The enthalpy values as calculated in Equation 32 do not include phase changes associated with condensation of water at the saturation point. This is a limitation of the model and the

quality will be lower for such conditions. The quality was used to indicate when conditions in the membrane system became non-ideal for the model, which would also suggest conditions in which condensation would occur inside the membrane. In most other cases the quality metric was above 90%, suggesting good heat exchange efficiency and ideal conditions within the membrane system.

Many of the results presented below are shown in psychrometric charts. These charts were obtained through Microsoft Excel psychrometric functions that come as add-ons to the program. In these charts, the y-axis shows the humidity weight ratio of water in air; this is often also referred to as water content. The x-axis is the dry bulb temperature of the air, as would be read by a thermometer. The relative humidity is also shown as curves that drop from the upper right-side of the graph to the lower left-side. The relative humidity is related to the partial pressure of water to the saturation partial pressure of water at the same temperature. Saturation is when water vapor is so concentrated at the given conditions that it can no longer remain as vapor and begins to condense. Other data can be reported with a psychrometric chart including: enthalpy, specific volume, and wet-bulb temperature. Psychrometric charts are shown at an atmospheric pressure of 76cmHg.

The data reported in the following psychrometric charts show the treatment of the membrane system from feed conditions to retentate conditions. The feed and retentate conditions are labeled in the first graph: Figure 12. This is comparable to Figure 5 above in which the red curve represented treatment done on the air stream by the membrane system. The blue curve in the figure represented treatment done by the DX-evaporator, and the green curve was treatment by the DX-condenser. The simulated results below do not show the DX treatment on the psychrometric charts, just the membrane system's treatment effect, even though all three treatment steps do occur.

Effect of Outdoor conditions

It may be intuitive to believe that membrane performance would be directly dependent on outdoor air conditions: temperature and humidity. To quantify the effect of outdoor conditions on membrane performance, simulations were conducted by varying first the outdoor humidity

level keeping the temperature constant, and then the outdoor temperature was varied while keeping the humidity constant. The results are presented in Figure 12-Figure 15.

For simulations where the feed temperature was constant, the feed temperature was held at 95°F while the outdoor relative humidity was allowed to vary between 74 and 94%. The results are presented in Figure 12.

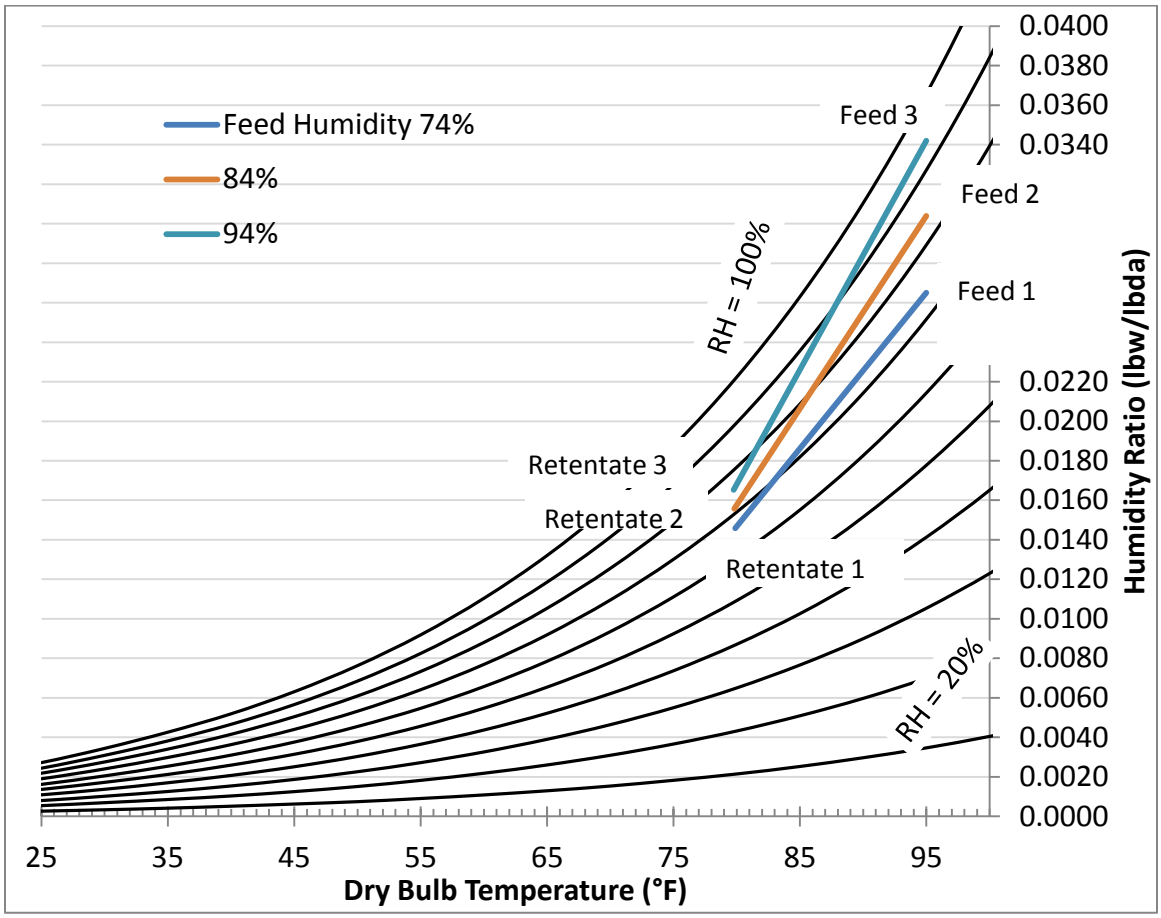

Figure 12: Comparing outdoor humidity levels to the membrane performance by using a psychrometric chart. Feed temperature is constant at 95°F. All other parameters are at base levels (see Table 5).

Figure 12 shows that the outdoor relative humidity level appears to have some effect on the conditions of the retentate stream. The retentate temperatures only vary by about 3°F, while the retentate humidity varies by less than 10% between the simulations shown. This implies that the outdoor humidity level is not a prime factor in the performance of the membrane system.

The relative energy savings resulting from these simulations are shown in Figure 13 for which there is only a 5% range of relative energy savings between all three humidity levels. From this, we can determine that the outdoor humidity level that is used as feed to the membrane has only a little effect on the energy savings.

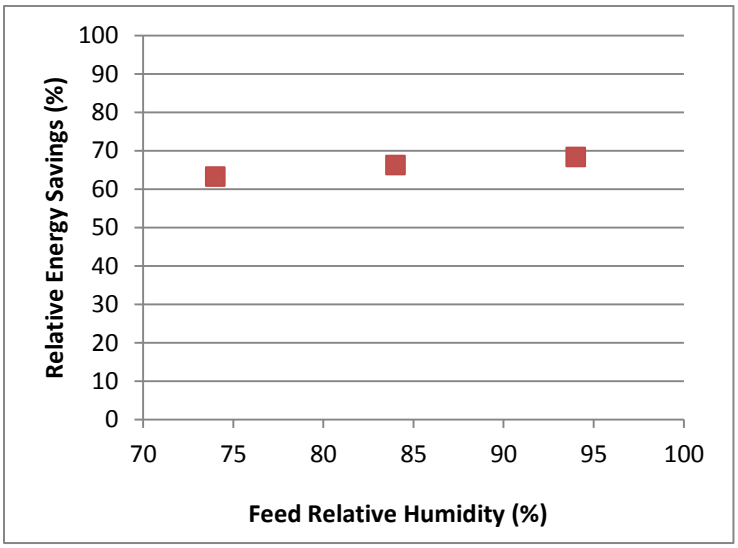

Figure 13: Relative energy savings of several feed humidity levels at a feed temperature of 95°F. All other parameters are at base levels (see Table 5).

Both Figure 12 and Figure 13 show that feed humidity has a minor influence on the retentate conditions and energy savings of the hybrid system. This is most likely because the contribution of the humidity level, or water molar fraction, in the feed does not have a large contribution to the feed partial pressure. A mathematical representation of this is shown in Equation 2 which is the molar flow of water through the membrane at step "i". This depends on the area of the discretized membrane fiber, a, the permeability coefficient of water, D_a, the thickness of the membrane, t, the feed pressure, pf, and the purge pressure, pp. The term x(i) is the water molar fraction in the feed at step "i", while y(i) is the molar fraction on the corresponding purge side.

$$wa(i) = a \cdot \frac{D_a}{t} \cdot (pf \cdot x(i) - pp \cdot y(i)) \tag{2}$$

The molar fractions of water in Equation 2 on the feed and purge sides are directly related to their humidity ratios. A low feed humidity will mean that x(i) is small. If y(i) remains

constant, then the value obtained by subtracting pp*y(i) from pf*x(i) will became larger for larger values of x(i), and therefore wa(i) will be larger. Thus separation of water from the feed will be better for a higher feed humidity. A feed humidity of 94% corresponds to a feed molar fraction of 0.049, while a humidity of 74% is a mole fraction of 0.038. Therefore, the difference in x(i) is small and the difference in pf*x(i) is small. These simulations show that the feed humidity has only a little effect on the membrane performance and energy savings.

The outdoor air temperature was also investigated from temperatures ranging from 85-105°F under a constant humidity level of 85%. The results are shown in Figure 14.

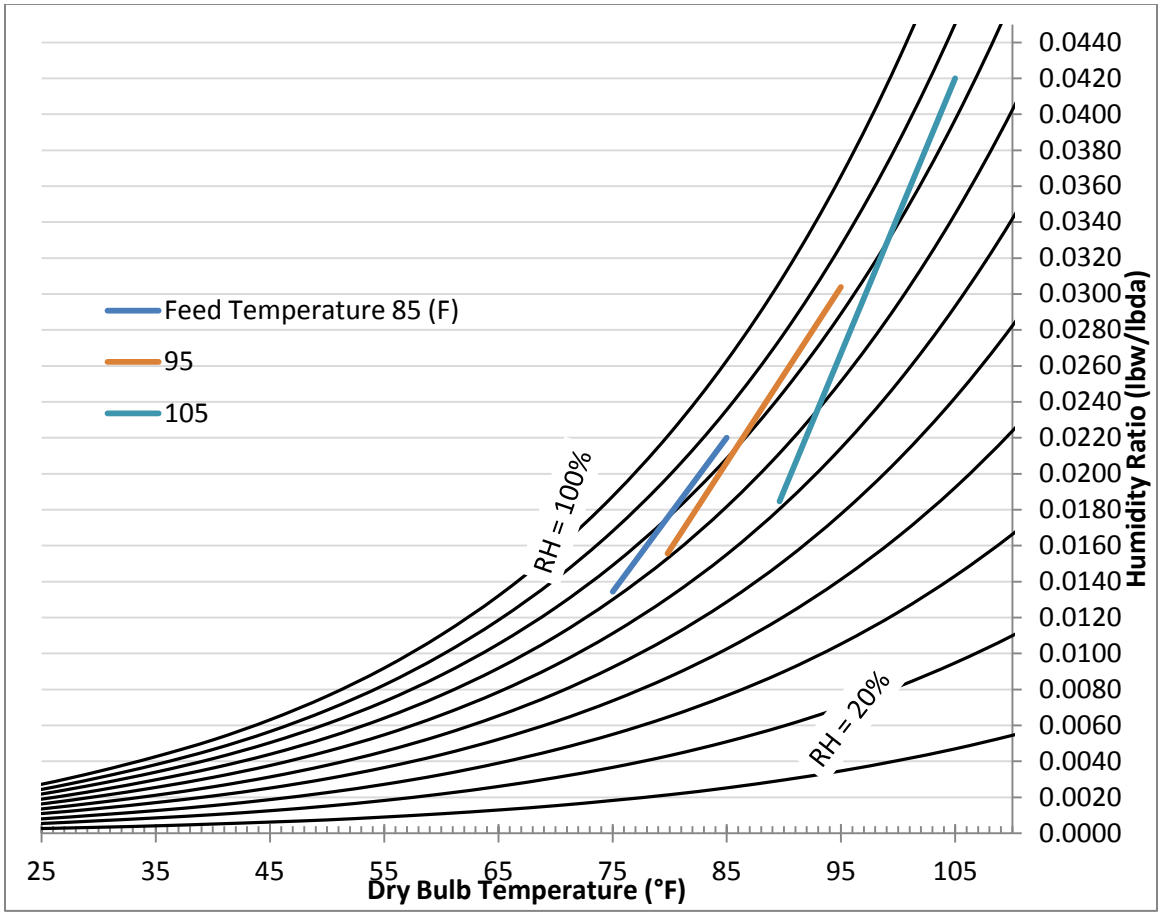

Figure 14: Psychrometric chart for feed streams of variable temperature, keeping humidity of feed constant at 85%. All other parameters are at base levels (see Table 5).

Figure 14 shows that the feed temperature has a strong influence on the retentate conditions; a small influence on the humidity, with a range of 10%, but a much larger influence on the temperature which ranges from 75-89°F. From Figure 14 it appears that the feed

temperature has a very strong effect on the membrane's performance. For the relative energy savings, a range of about 9% was found as shown in Figure 15.

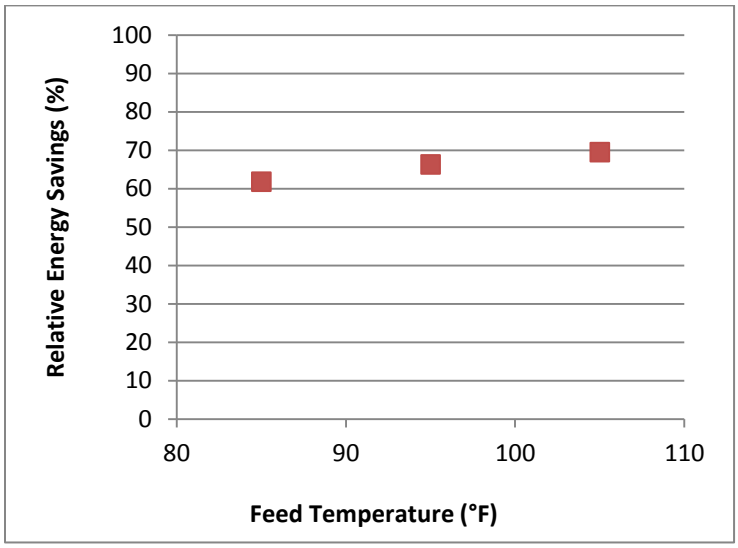

Figure 15: Relative energy savings of varying feed temperature. All other parameters are at base levels (see Table 5).

Figure 14 and Figure 15 show how differences in retentate conditions affect the energy savings due to changing the cooling load required by the DX part of the system. These results may be explained by the changes between the specific energy and the latent energy of the retentate stream. Although the temperature of the retentate in each simulation is strongly affected by outside temperatures, the humidity of the retentate ranges only by about 10%, which is a range of 0.005 in the molar ratio of water over air; a small change in water content. Water content and humidity are associated with the latent energy of the retentate. Since the retentate streams' molar fraction of each case is close in value, their latent energies are also roughly equal. The DX part of the hybrid system treats the retentate air to the desired 40% humidity and 68°F temperature and energy requirements are associated with the latent and specific heats of the retentate. Because the latent heats of the retentate streams in each case do not differ by a large amount, neither does the latent energy of the DX treatment. Because cooling of the retentate to the saturation point for all cases is roughly the same (10-15°F) the specific heat of cooling via DX treatment is also nearly identical for each case. This is the most likely reason why the energy savings in Figure 15 have a moderately strong relationship with the feed temperature.

Effect of Purge conditions

Similar to the feed conditions, the purge conditions were investigated to determine their influence on the membrane's performance. Purge humidity levels were varied between 50 and 70% at a constant temperature of 75°F. The results of these simulations are shown in Figure 16.

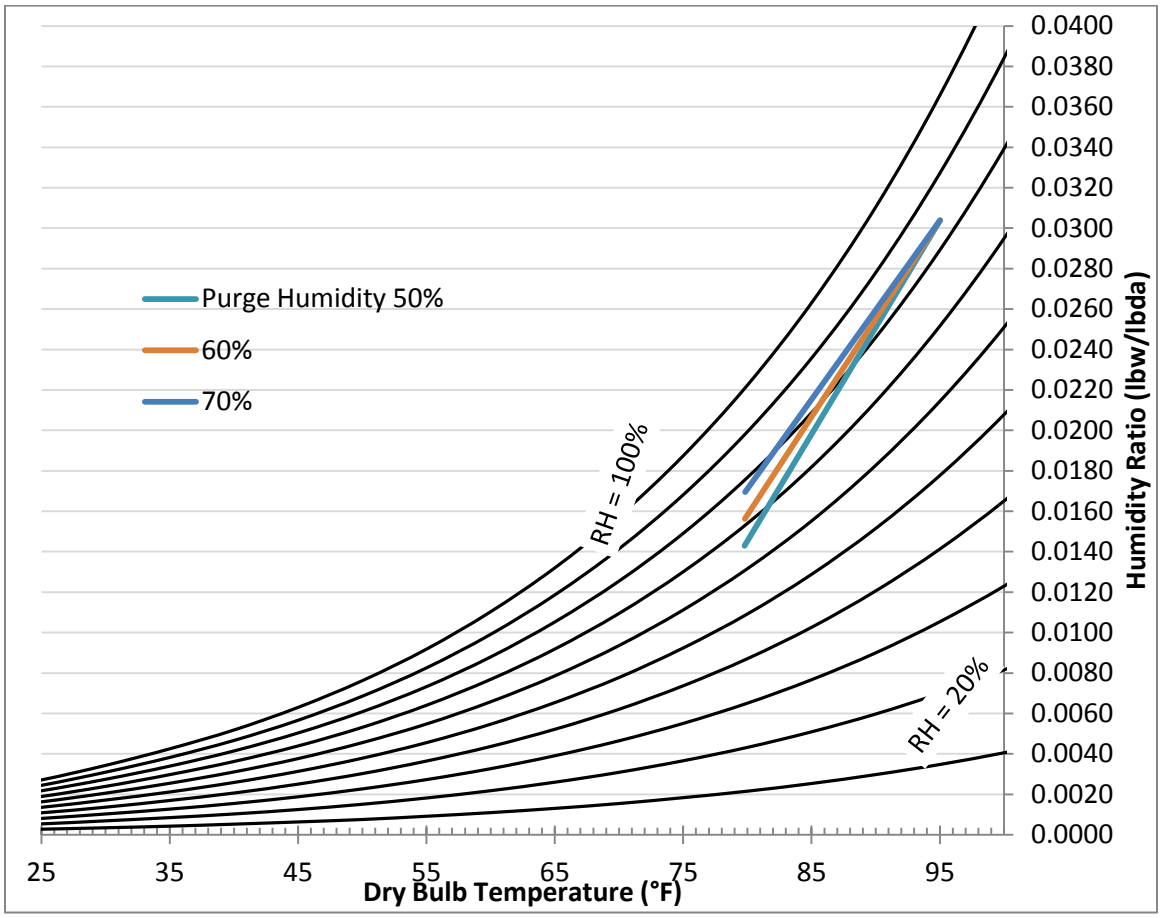

Figure 16: Effect of purge relative humidity at constant temperature of 75°F. All other parameters are at base levels (see Table 5).

The results in Figure 16 suggest that the humidity of the purge flow rate has an influence on the retentate. The retentate humidity ratio decreases with decreasing purge humidity. This is because moisture transfer is greatest for a large difference between feed humidity and purge humidity. The trend in Figure 16 can be mathematically explained by re-examination of the flux equations used in the model and described in Chapter 2. Equation 2 is the molar flux of water through the membrane at step "i". This depends on the area of the discretized membrane fiber, a,

the permeability coefficient of water, D_a, the thickness of the membrane, t, the feed pressure, pf, and the purge pressure, pp. The term x(i) is the water molar fraction in the feed at step "i", while y(i) is the molar fraction on the corresponding purge side.

$$wa(i) = a \cdot \frac{D_a}{t} \cdot (pf \cdot x(i) - pp \cdot y(i)) \quad (2)$$

The molar fractions of water in Equation 2 on the feed and purge sides are directly related to their humidity ratios. A low purge humidity will mean that y(i) is small. If x(i) remains constant, then the value obtained by subtracting pp*y(i) from pf*x(i) will became larger for smaller values of y(i), and therefore wa(i), the flow of water through the membrane, will be larger. Thus separation of water from the feed will be better for lower purge humidity.

The relative energy savings of these simulations are shown in Figure 17 which demonstrates that the energy savings decrease with increasing purge humidity. Figure 17 shows that energy savings have a range by almost 7% for the simulated purge conditions.

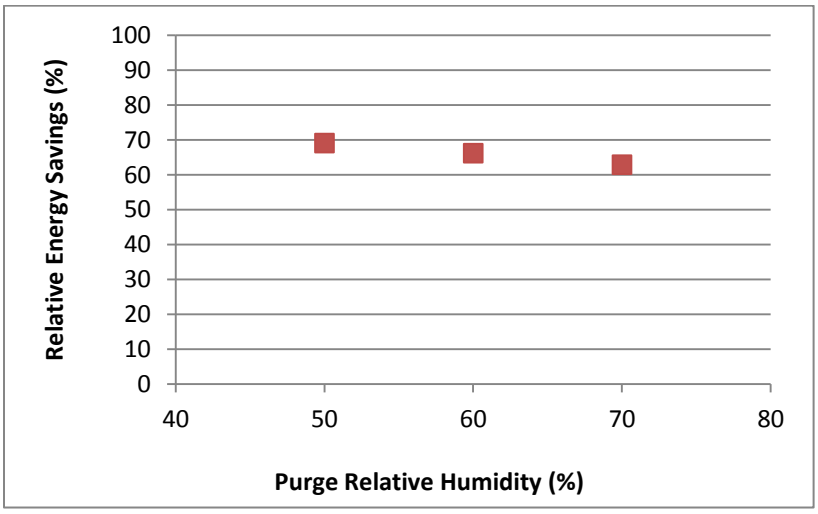

Figure 17: Relative energy savings for several purge humidity levels. All other parameters are at base levels (see Table 5).

The trend in Figure 17 is directly related to the trend in Figure 16, which shows decreasing water content with decreasing purge humidity. The relation between these two graphs shows that energy savings are greater for purge streams with lower humidity. This can be attributed to the latent and specific energies of the retentate stream. Since the retentate streams' humidity of each case is close in value, their latent energies are also roughly equal. The DX part

of the hybrid system treats the retentate air to the desired 40% humidity, latent energy change, and 68°F temperature, a specific energy change. Because the latent heats of the retentate streams in each case do not differ by a large amount, neither does the latent energy of the DX treatment. Because cooling the retentate to the saturation point ranges from 10-15°F the specific heat of cooling has some effect on the DX energy requirements, though not much. Thus, energy savings will be moderately affected by changing the purge humidity.

The effect of the purge temperature was also simulated by varying the temperature from 65-85°F. The results are shown in Figure 18.

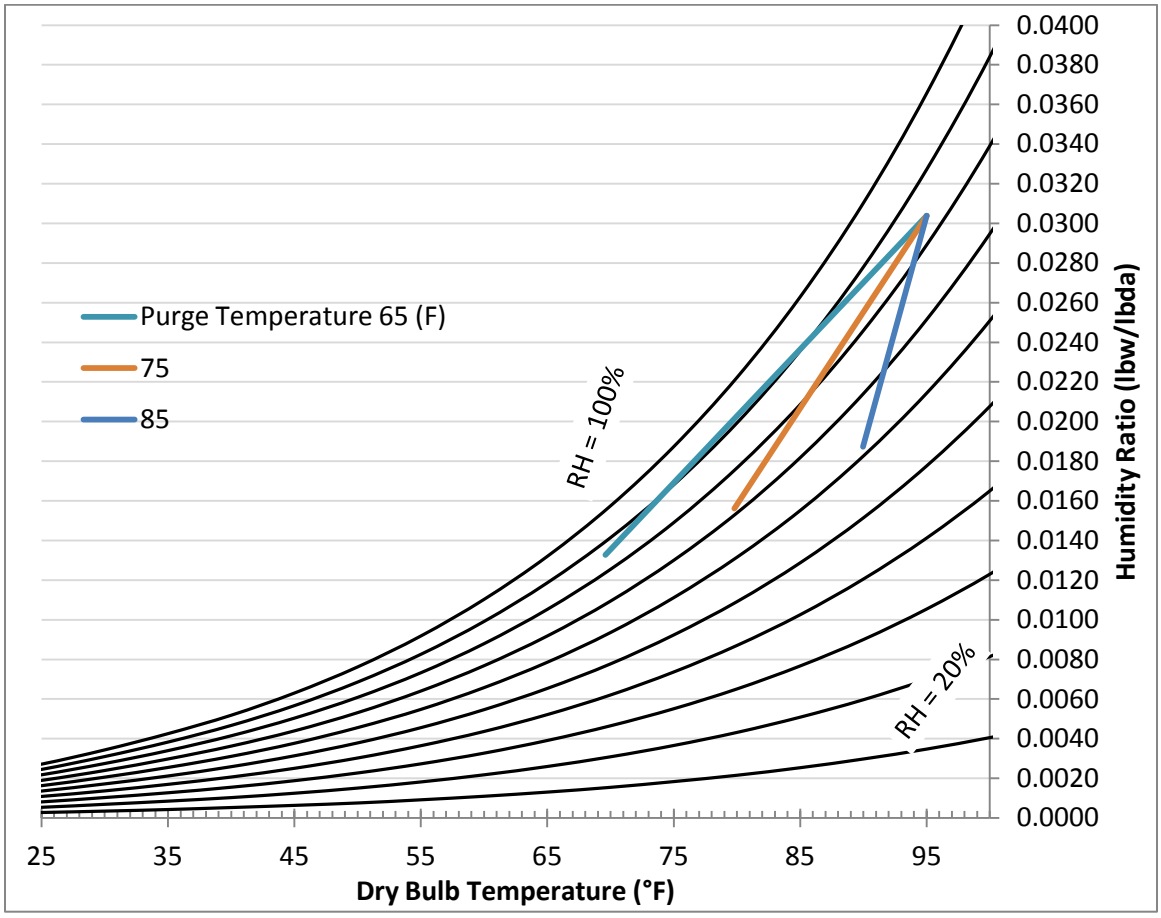

Figure 18: Psychrometric chart of the effect of changing the purge stream temperature. All other parameters are at base levels (see Table 5).

The purge temperature has a great effect on the retentate temperature. This is because the purge temperature is the minimum possible temperature that can be obtained by the retentate; decreasing the purge temperature will decrease this minimum. In mathematical terms, the energy

flow from the hot feed side to the cold purge side is shown by rearranging and simplifying Equation 18 into the equation shown below:

$$q(i) = \left(T_{hot} - T_{cold}\right)\cdot\left(F(i)\cdot cp_h\right) \tag{18}$$

The important term to notice here is the subtraction of T_{hot} with T_{cold}. The flow of energy, q(i), will be greater for smaller values of T_{cold}. The flow of energy is related to the amount of heat transfer that occurs between the feed (hot) and purge (cold) side of the membrane. Since the model works on the assumption of perfect heat transfer within the membrane, all the heat that is lost between the feed and retentate will be gained between the purge and exhaust. A greater amount of heat transfer occurs for smaller values of T_{cold} such that the heat lost on the feed side is greater and therefore the retentate temperature is decreased accordingly as shown in Figure 18.

The energy impact of this behavior is shown in Figure 19 which illustrates that energy savings are very affected by the purge temperature, with a range of about 24%.

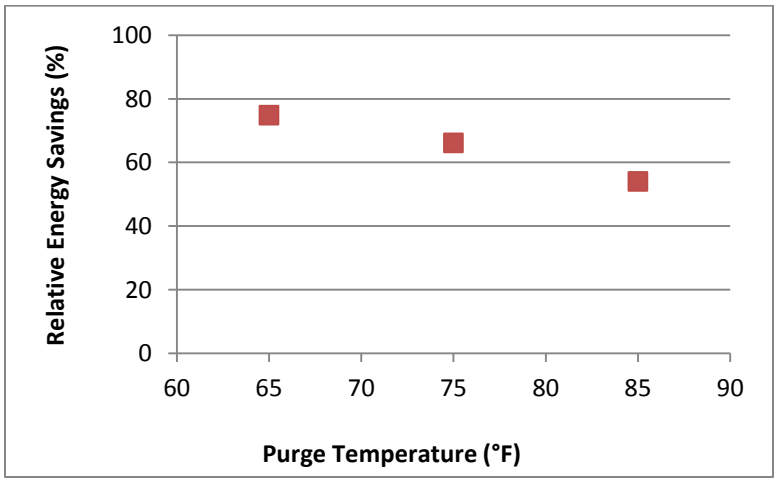

Figure 19: Trend of relative energy savings with varying purge temperature. All other parameters are at base levels (see Table 5).

The retentate humidity from simulations in Figure 18 has a range of over 25%. This means that the energy requirements for the DX-evaporator associated with latent and specific enthalpies greatly vary by varying the purge temperature. For high purge temperatures, the evaporator has a high specific energy cost to lower the retentate temperature in addition to a greater latent energy cost required for condensation of the higher water content of the retentate. Low purge temperatures cause the retentate to be colder and already closer to the saturation point

such that the DX-evaporator has less cooling load, by a significant amount, and therefore less energy requirement.

Investigation of the purge conditions is novel to this study. Even though previous studies investigated the outdoor air conditions, little has been said of the purge conditions (Bergero 2011). The results presented here show that the purge, or indoor air conditions have a larger effect on energy savings than the outdoor air conditions.

Thickness

The thickness of the membrane will affect the resistance of the vapor flux through the membrane. A thinner membrane should have a greater flow, and therefore a faster transport of water, than a thicker membrane. This is shown mathematically in the flowequation, Equation 2, reprinted below:

$$wa(i) = a \cdot \frac{D_a}{t} \cdot (pf \cdot x(i) - pp \cdot y(i)) \tag{2}$$

The flow of water is inversely proportional to membrane thickness. Indeed, this is the trend that was observed for simulations with varying membrane thickness as shown in Figure 20. Membrane thicknesses are often smaller than those reported in Figure 20. Asymmetric membranes can be smaller than 1μm, while the thickness reported by Zhang's liquid membrane was 142μm (Zhang Xiao 2008). Using a thickness less than 15μm the model was unable to converge without changing baseline conditions, such as increasing the flow rate, or changing the number of discretizations along the fibers. To avoid changing the baseline conditions the judgment was made to report thicknesses at 15μm and higher.

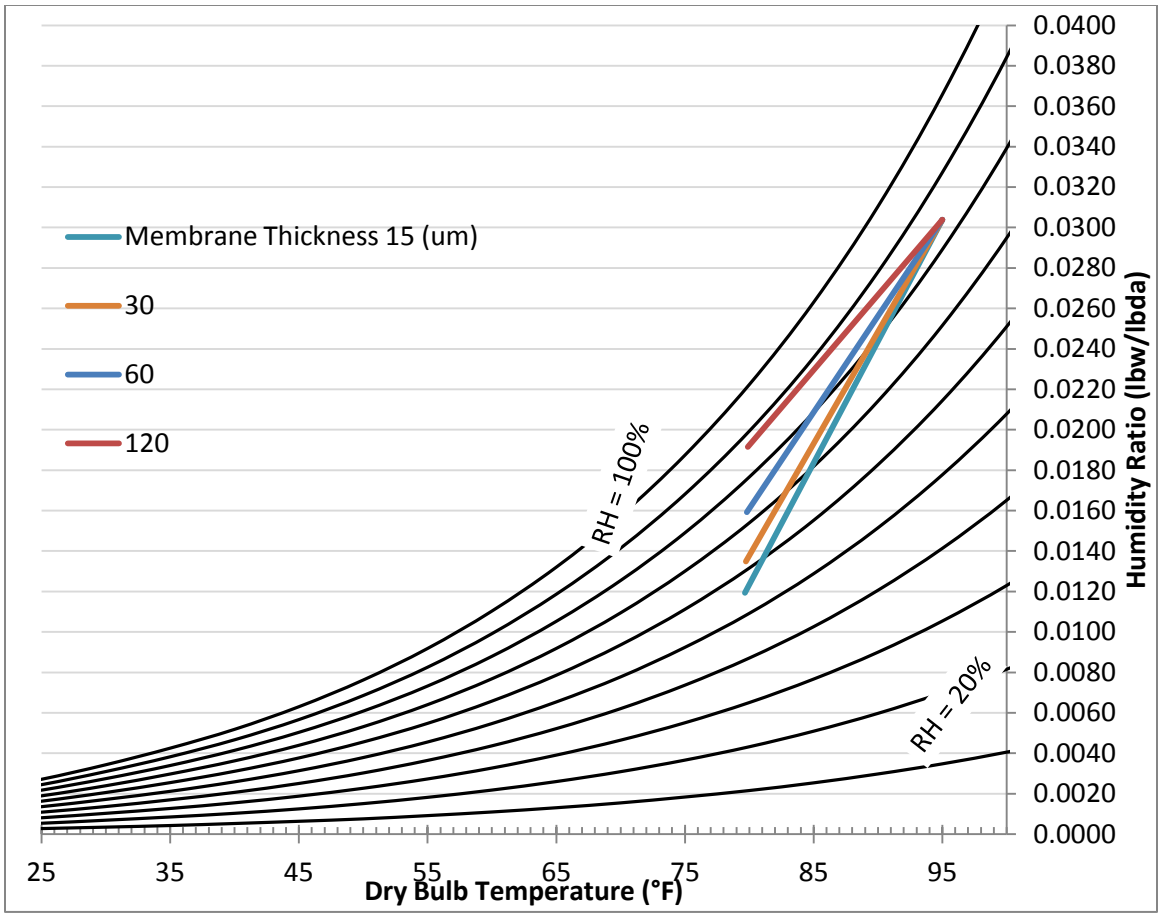

Figure 20: Psychrometric chart for several membrane thicknesses on the dehumidification of air. All other parameters are at base levels (see Table 5).

The separation of water from air increases with decreasing thickness. It is important to note that the thickness of a membrane is defined by the thickness of its selective layer. For very thin membranes, mechanical integrity may be compromised and a support layer is needed. This is called an asymmetric membrane as described in Chapter 2. Different polymeric materials have different thickness minimums they can withstand before requiring a support substructure. This should be a consideration when choosing a membrane material for these AC hybrid systems.

From inspection of the trend in Figure 20 one would intuitively predict that the energy savings will decrease with increasing thickness. Indeed, this is so as shown in Figure 21.

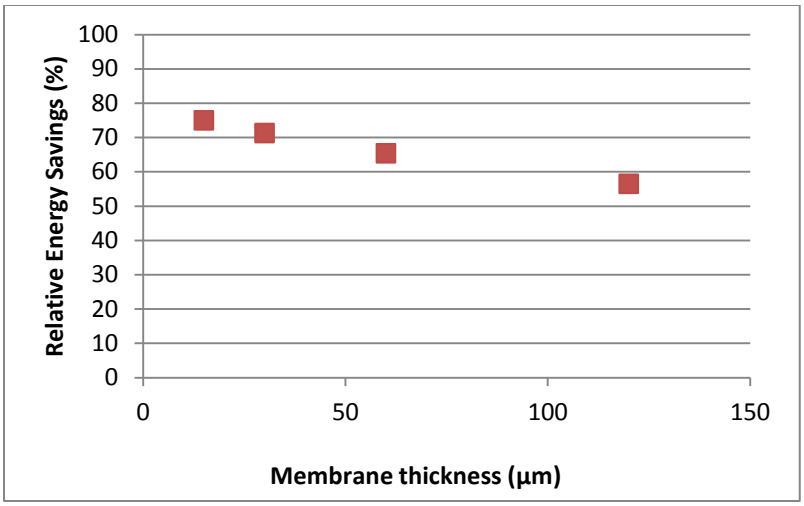

Figure 21: Relative energy savings of varying membrane thickness. All other parameters are at base levels (see Table 5).

The decrease in relative energy savings with increasing thickness is a direct correlation to the decrease in the flow of water across the membrane that is caused by the inverse relationship with membrane thickness according to Equation 2. This trend suggests that asymmetric membranes with thicknesses less than 1µm will have even larger energy savings than the values shown in Figure 21.

A fifth simulation was run for a thickness of 1µm, which convergence was reached at a feed flow rate of 0.02 mol/s, ten times higher than the baseline, 600 iterations, and discretizing the fibers into 400 pieces rather than the usual 100. Note that choice of the feed flow rate is a module design parameter, for the MedArray module, this was limited to 0.002 mol/s, but using a different module design could allow for higher flow rates. This fifth thickness simulation showed energy savings of 77%, not shown in Figure 21. Thickness and area both have an impact on the productivity of the membrane system. This concept will be discussed further in the next section.

Area

The membrane area was next simulated, results are shown below. It is important to note that the areas simulated here are quite small. This is because the flow rates that are modeled are also small. To give an idea of scale, the MedArray module used in these simulations has a suggested maximum air flow rate of 0.002 mol/s of air for an area of 2500cm^2, whereas Zhang's

(Zhang 2012) module is $8m^2$ ($80{,}000cm^2$) and has an average air flow rate of $200m^3/h$ (2.7 mol/s) [3]. These numbers mean that Zhang's module has an area 32 times larger than the ones in this simulation while as the flow rate is over 1000 times greater. However, this does not mean that the productivity of Zhang's membrane is higher than the MedArray membrane used for these simulations. Zhang's flat plate membrane lowered the humidity ratio of the feed by 0.0182 moles of water per mole of air, while the MedArray module lowered the humidity ratio by 0.027 moles of water/ mole of air. Due to flow rates, Zhang's membrane system was able to separate $6.14x10^{-7}$ mol $H_2O/s/cm^2$. A simulation run at a thickness of 1μm, discussed above, had a separation of $2.13x10^{-7}$ mol $H_2O/s/cm^2$ which is comparable to Zhang's separation productivity; while the MedArray module with a thickness of 15μm separated $2.12x10^{-8}$ mol $H_2O/s/cm^2$. This further demonstrates the inverse relationship that thickness has on the performance of the membrane; decreasing the thickness by a factor of 10 increased the membrane system productivity by a factor of 10. Furthermore, the membrane with a thickness of 1μm is close to Zhang's productivity results even though the flow rates and areas are several orders of magnitude different.

The effect of the area on the separation of water is shown in the psychrometric chart below in Figure 22.

[3] Zhang's air flow rate is large enough to provide treated air to a room with floor space of 200 square meters (Zhang 2012); this is roughly the size of a small shop or a large apartment.

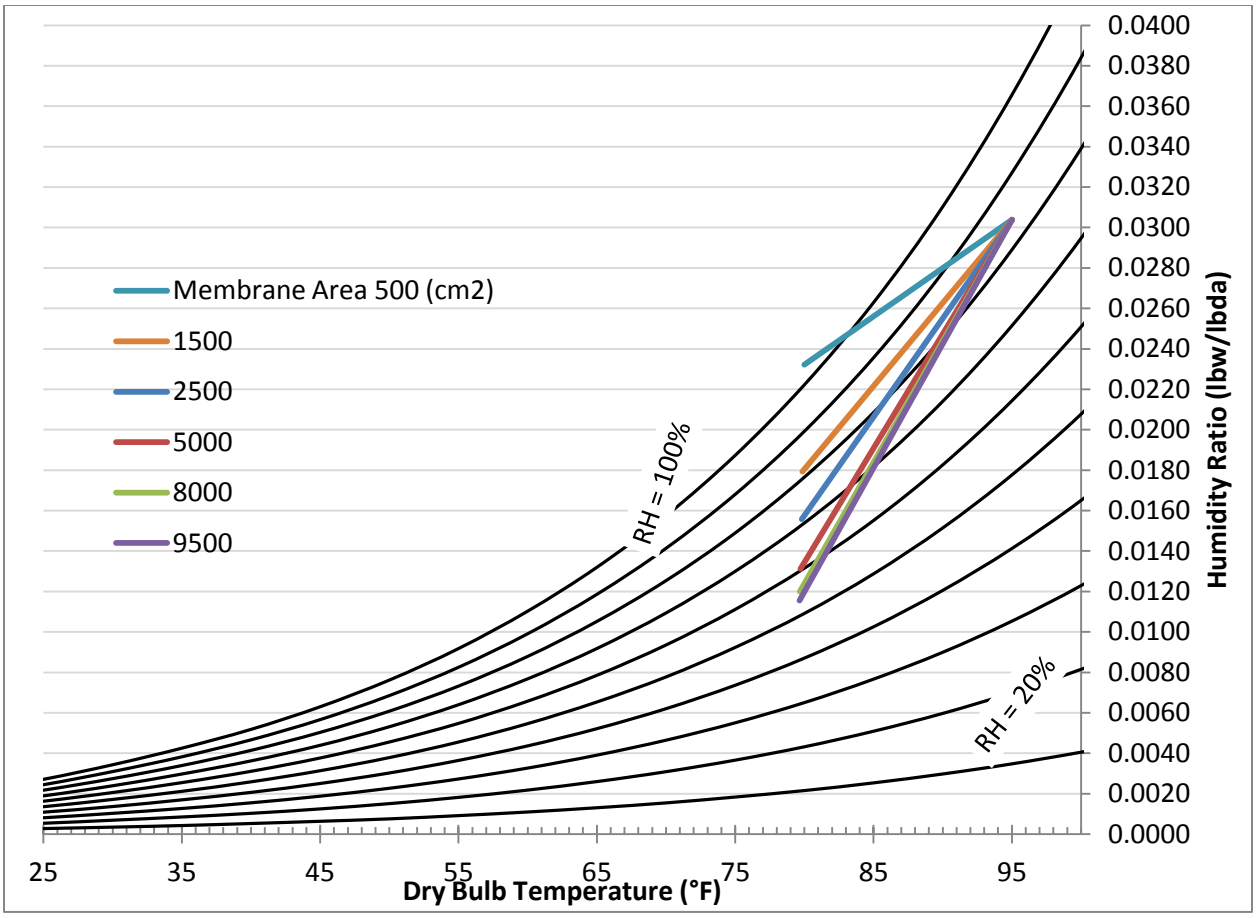

Figure 22: Psychrometric chart for the separation of water from air for membranes of differing area. All other parameters are at base levels (see Table 5).

Figure 22 shows the trend that an increased membrane surface area gives more water separation. However, the advantage of this effect becomes almost negligible between areas of 5000 and 9500cm^2. In fact, such little difference in dehumidification with such a large increase in area would actually be disadvantageous. The material cost of the extra membrane area will not outweigh the extra monetary energy savings for areas larger than 5000cm^2. This means that there is an optimal membrane area associated with energy and performance. At a membrane area of 500cm^2, the retentate appears to cross the saturation line. Existence beyond the saturation point is a thermodynamic impossibility but is a mathematical cause due to limitations of the model.

A mathematical explanation of Figure 22 can be given from inspection of Equation 3 shown below. Equation 3 is the total molar flow of both water and air. The term wa(i) is the water molar flow across the membrane, and is described by Equation 2 which was discussed

previously. The air molar flow is the second, larger term involving the permeability of air, Db, the membrane area, a, the membrane fiber thickness, t, the feed pressure, pf, the purge pressure, pp, and the air mole fractions on the feed side, (1-x(i)), and purge side, (1-y(i)).

$$W(i) = wa(i) + a \cdot \frac{D_b}{t} \cdot [pf \cdot (1 - x(i)) - pp \cdot (1 - y(i))] \quad (3)$$

Here in Equation 3 the membrane area is actually the discretized area between step "i" and "i+1". The value of "a" is calculated by dividing the total membrane area by the number of discretized pieces chosen for modeling (called "n" this number was consistently 100). Regardless of terminology, if the total membrane area is increased, the total flow will also increase due to the flow's direct, linear proportion with area. This is why the separation of water in Figure 22 increases with increasing area.

Figure 23 shows the relative energy savings of these simulations. The relative energy savings appear to plateau at an area of 5000cm^2. This is because the increased area also increases the amount of air that permeates the membrane. This means the retentate flow rate decreases as membrane area increases due to permeation of air in addition to permeation of water. The retentate flow rate, or the delivered air, directly affects the relative energy savings by the mathematical definition in Equation 31. This further indicates that there is an optimal membrane area, beyond which loses any advantage.

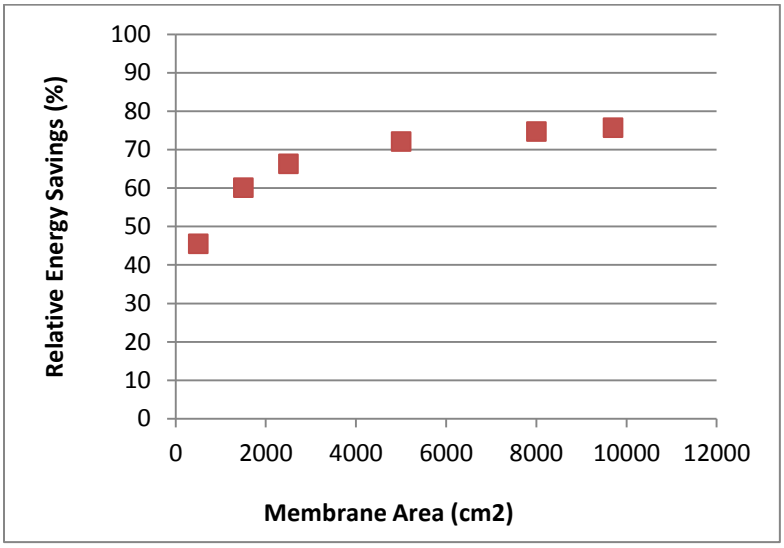

Figure 23: Relative energy savings with varying membrane area. All other parameters are at base levels (see Table 5).

Membrane area is a description of the surface area of the selective polymer. A large surface area can be packed inside a comparatively small module. This is useful for questions regarding size requirements for installation of a membrane module with a pre-existing DX system. Due to increasing the area, air will increasingly permeate through the membrane and cause the retentate flow rate to lower. This ultimately means that there is an optimum area that should be chosen for the process.

Feed Pressure

Another system property that has never before been investigated with regard to membrane total heat exchangers is the pressure. The driving force for gas permeation is directly related to the pressure difference between the feed and purge sides of the membrane, as shown by the flow equation. Equation 2 is the flow of water through the membrane and is copied below:

$$wa(i) = a \cdot \frac{D_a}{t} \cdot (pf \cdot x(i) - pp \cdot y(i)) \tag{2}$$

The terms pf and pp describe the feed and purge pressure respectively. The terms x(i) and y(i) are the water molar fraction on the feed side and purge side respectively. The product of pf*x(i) is the partial pressure of water on the feed side at step "i", while the product of pp*y(i) is the corresponding partial pressure of water on the purge side. The difference between the two has a direct relation to the molar flow of water and is the major driving force. Equation 3 in the previous section contains a term which describes the same relationship for the flux of air.

Different technologies have limits to what pressures can be provided. Fans have an upper limit of 84cmHg (or 8cmHg above atmospheric pressure) while compressors can provide any pressure (Bureau 2013). Since the pressure range of fans is small, it is possible to assume the specific heat capacity of air is constant and that the fan does not cause an increase in temperature due to the increase in pressure. However, compressors do increase air temperature with increases in pressure. This is shown by the adiabatic compression of an ideal gas in Equation 33.

$$\frac{T_2}{T_1} = \left(\frac{P_2}{P_1}\right)^{\frac{R}{C_p}} \tag{33}$$

Equation 33 shows the relationship between temperature (T_1, T_2) and pressure (P_1, P_2) at two different states, one state at the inlet of the compressor and one state at the outlet of the compressor. R is the universal gas constant; C_p is the specific heat capacity of air. By increasing one pressure, the corresponding temperature will also increase. Thus, increasing the feed pressure by using an air compressor will heat up the air stream. The overall energy requirement of the compressor is given by the following Equation 34. For which the enthalpy is a function of both the fraction of water in the air stream, the temperature, and pressure as is given by a psychrometric calculator function in Microsoft Excel 2011. Typical isentropic efficiencies of compressors are between 75-85% (University of Illinois 2008), for the purposes of this study an efficiency of 85% was used for the compressor.

$$\text{Energy}_{\text{Compressor}} = \left(\text{Enthalpy}_{\text{After.Compressor}} - \text{Enthalpy}_{\text{Before.Compressor}}\right) \cdot \frac{\text{Flowrate}}{\text{efficiency}_{\text{Compressor}}} \quad (34)$$

By Equation 2 above, the effect of increasing the pressure difference should cause an increase in water flux and separation. Indeed, this is the trend predicted by the model caused by changing the feed pressure and is shown by the chart in Figure 24. The simulations of feed pressures below 84cmHg use a fan to provide pressure, while the simulation above this pressure uses a compressor. As discussed above, the compressor heats up the air stream, marked in Figure 24 by the long blue horizontal line. This hot feed from the compressor is the feed into the membrane. Since the feed to the membrane is much hotter, the retentate is not able to be cooled below 115°F. Even though the temperatures are different between using a fan and using a compressor, the trend still holds that increasing the feed pressure increases water flux and lowers the humidity ratio of the retentate.

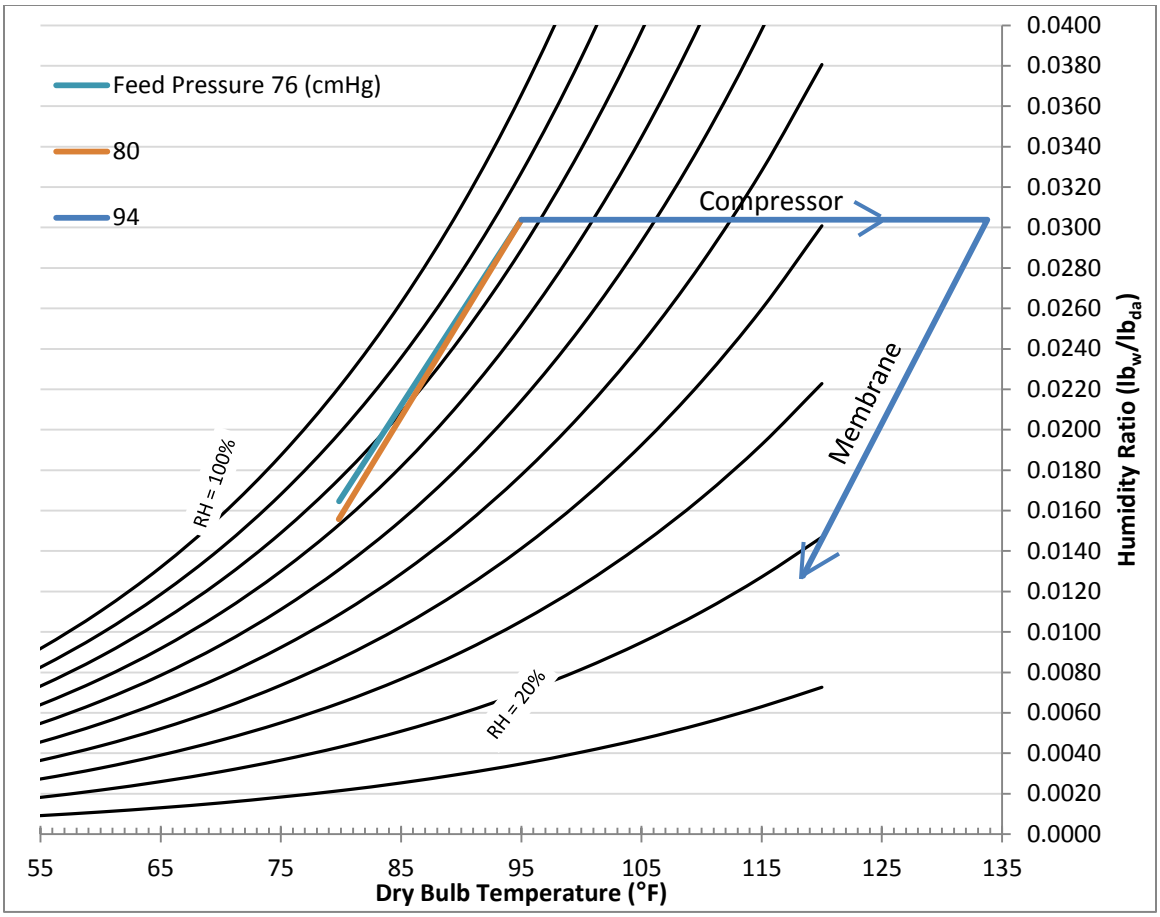

Figure 24: Psychrometric chart showing the effect of changing the feed side total pressure while keeping all other variables constant. Feed pressures below 84cmHg use a fan. The feed pressure of 94cmHg is supplied by a compressor. All other parameters are at base levels (see Table 5).

The energy savings relative to the delivery flow rate are shown in Figure 25. Note a feed pressure of 154 cmHg was also simulated that was not shown in Figure 24. This is because the compressor heated the feed stream to above 200°F which would not fit the scale in Figure 24.

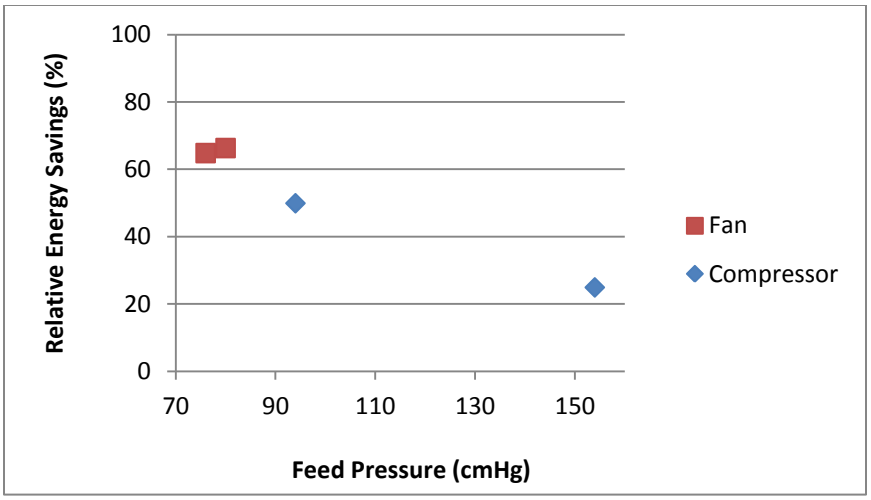

Figure 25: Relative energy savings with increasing feed pressure.

Figure 25 shows an increasing trend in energy savings with increasing feed pressure when using a fan. When using a compressor, increasing the feed pressure decreases the energy savings. This is because a fan does not heat air as it increases the pressure, a compressor does. The increase in the feed temperature is so high that the specific energy required to cool the resulting retentate is extremely large. Although increasing the feed pressure increases water flow across the membrane and results in a lower water content of the retentate, this latent energy benefit does not outweigh the specific energy costs required by the DX evaporator to cool the retentate. Though a compressor has this trend, a fan has the opposite. Increasing the feed pressure increases the energy savings. Since the feed temperature is not affected by a fan, the increase in water flux by increasing the pressure will have a latent heat benefit by lowering the humidity ratio of the retentate; this latent heat benefit translates to energy savings.

Purge pressure

As described in the previous section, the pressure difference between feed and purge is directly related to the permeation of water and air through the membrane. This is a concept that has, until now, not been investigated in regards to membrane total heat exchangers. Figure 26 shows the results of varying the purge pressure while keeping the feed pressure constant at 80cmHg.

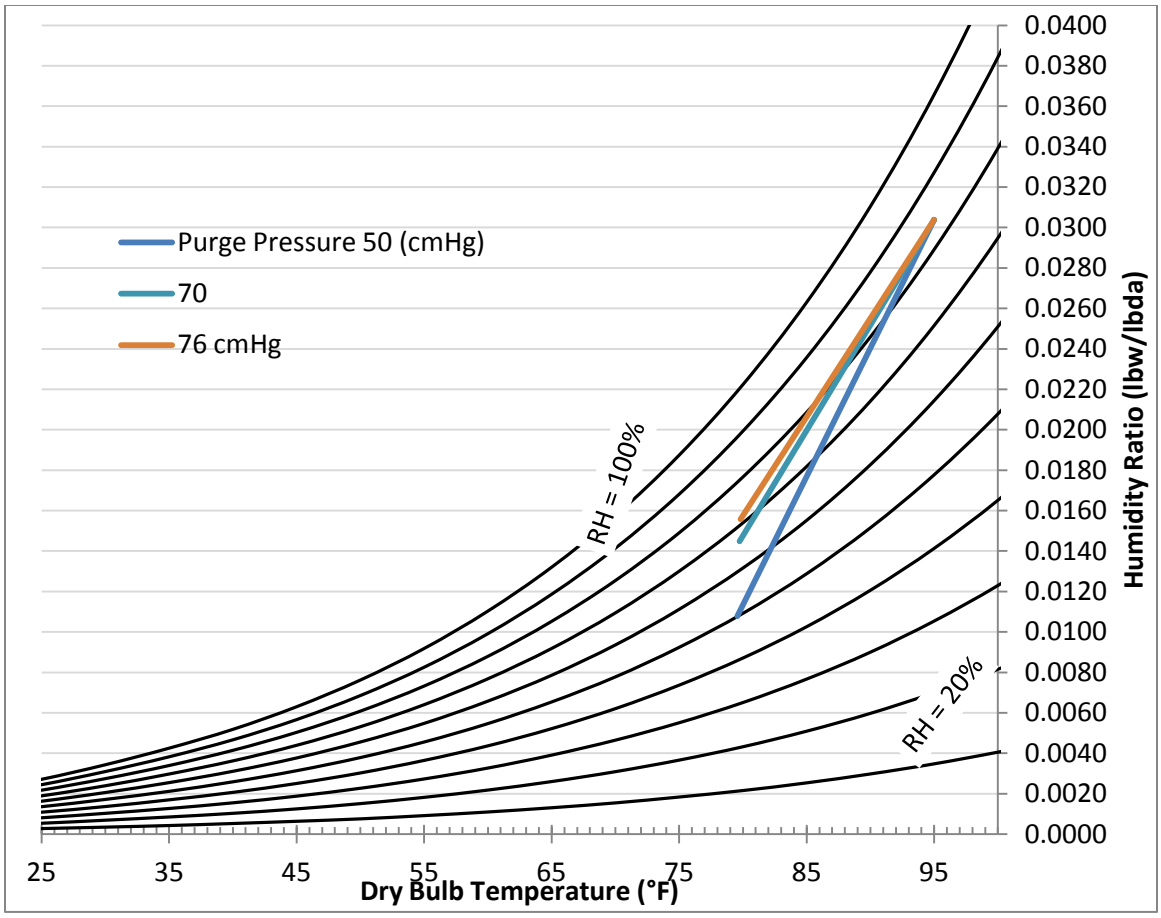

Figure 26: Psychrometric chart for the effect of purge pressure on membrane separation. All other parameters are at base levels (see Table 5).

Figure 26 shows that as the purge pressure increases, the removal of water decreases. Since pressures below 76cmHg are below atmospheric, a vacuum system must be used to provide these pressures. This is accomplished by placing the fan or compressor on the exhaust stream such that the purge is actually sucked through the membrane and exhausted out of the fan or compressor. A fan can supply a pressure within 8cmHg of atmospheric pressure (Bureau 2013) while a compressor can supply a vacuum. As described in the previous section a fan causes no temperature increase to its outlet stream, while a compressor does. The increase in gas temperature due to compression can be modeled by an adiabatic system on an ideal gas as shown above in Equation 33. This increase in temperature would increase the exhaust temperature leaving the membrane, not the temperature of the purge entering it.

Figure 27 further supports the conclusions stated before: that energy savings and separation are directly related to pressure difference. Decreasing the purge pressure with a fan increases the energy savings. However, using a compressor causes a savings decrease from using a fan.

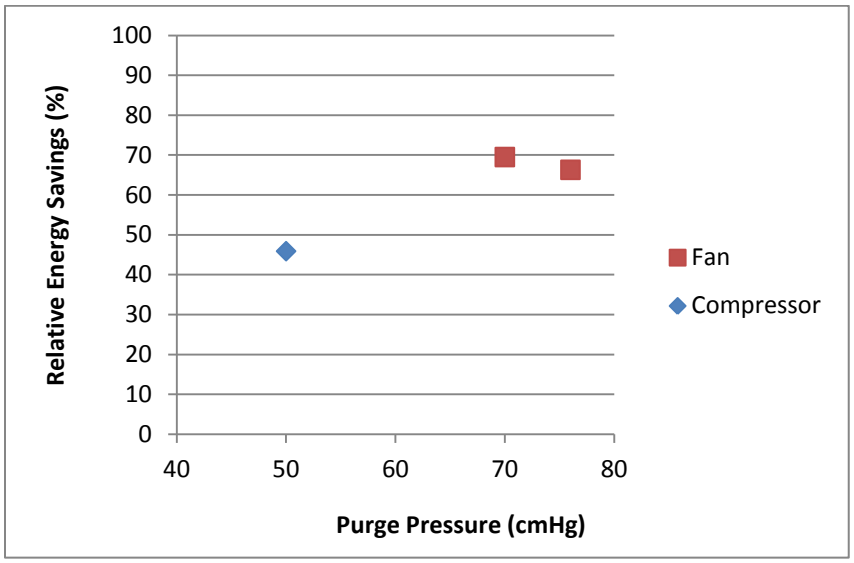

Figure 27: Relative energy savings of changing purge pressure. All other parameters are at base levels (see Table 5).

The lower energy savings due to using a compressor is related to the energy requirements of the compressor, rather than due to changes in energy requirements to treat the retentate. Although the retentate at low pressures has a low humidity ratio, this latent energy benefit does not outweigh the energy required by the compressor to operate at such pressures. Lower pressures require more energy from the compressor and therefore have lower energy savings. However, low purge pressures that can be obtained by a fan result in higher energy savings.

Flow Rates

The flow rate of the feed and the purge are investigated according to their ratios with each other. It is impractical for the purge flow rate to be greater than the feed flow rate. Laws of mass balances dictate that the supply of air into a room must equal the flow out of the room in order to maintain equilibrium conditions within it. Conversely, it is reasonable for the purge flow to be less than the feed flow, because the indoor air for AC systems is already exhausted; not all

indoor air needs to be used as the purge. Thus, increasing the feed flow from a 1:1 ratio with the purge flow to four times higher was used for simulations. The results are shown in Figure 28.

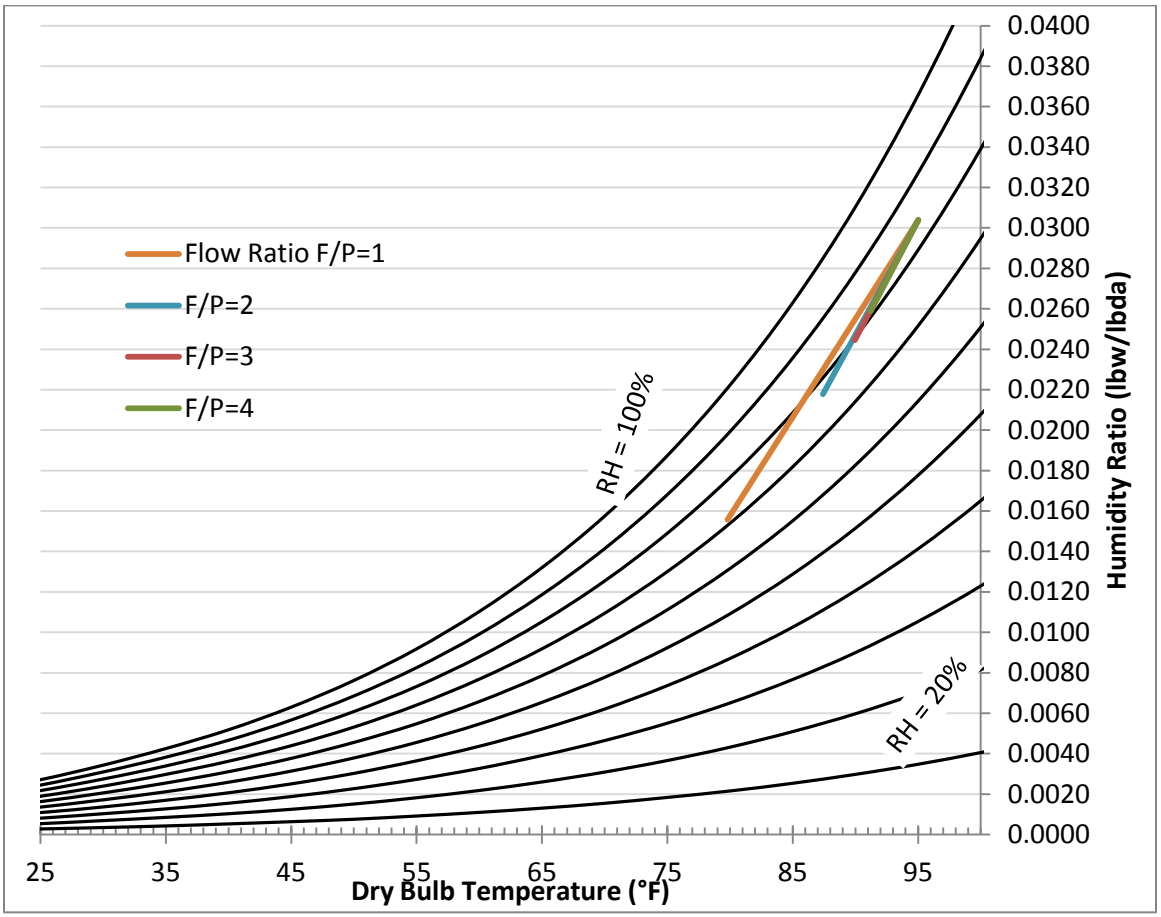

Figure 28: Effect of varying feed and purge flow rates. All other parameters are at base levels (see Table 5).

It appears in Figure 28 that better dehumidification occurs for lower feed to purge flow ratios, or for higher purge flow rates. This is because the purge is essentially stripping and carrying away the water content from the feed. Furthermore, a higher purge flow rate corresponds to a greater horizontal shift of the curves in Figure 28 indicating better heat transfer. This is mathematically based on the relationship of feed and purge heat flux with their flow rates shown by modified versions of Equations 18 and 19 respectively below.

$$q(i) = \left(T_{feed}(i) - T_{feed}(i+1)\right)\cdot\left(F(i)\cdot cp_h\right) \quad (18)$$

$$q(i) = \left(T_{purge}(i+1) - T_{purge}(i)\right)\cdot\left(P(i)\cdot cp_c\right) \quad (19)$$

The heat flux lost by the feed is equal in magnitude and opposite in direction to the heat flux gained by the purge. Both of these heat fluxes depend on their respective flow rates in a directly proportional relationship as evidenced by the two equations shown above. A higher purge flow rate means that the heat gained on the purge side is larger, and therefore the heat lost by the feed is larger, and the retentate temperature is lowered.

Figure 29 shows the energy analysis of these simulations for which the relative energy savings decrease with decreasing purge flow (increasing feed to purge ratio). The energy trend shown is caused because both heat and moisture transfer are diminished with decreasing purge flow rate.

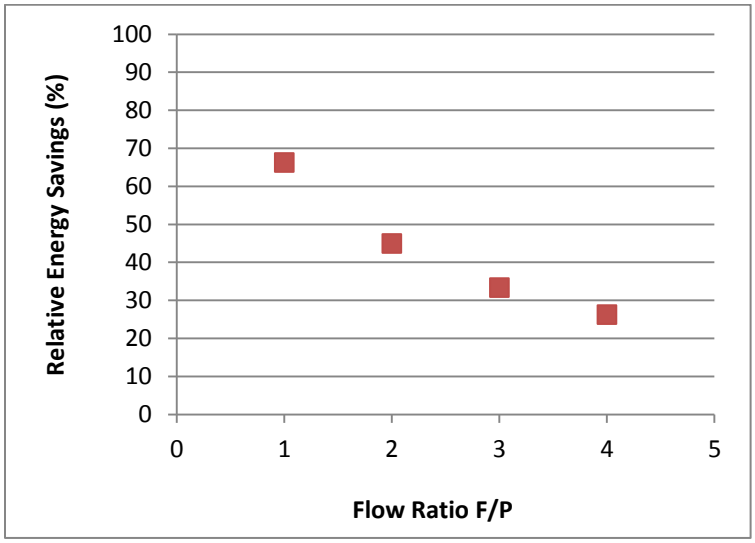

Figure 29: Relative energy savings of changing flow rates. All other parameters are at base levels (see Table 5).

The range of energy savings is 40% in Figure 29 showing that the relationship between flow rates and energy savings is a strong one. This is not only due to the mathematical relationship described above, but relates to the latent and specific energy requirements by the DX part of the hybrid system to treat the retentate to 40% humidity and 68°F. The retentate humidity has a range of over 10% in Figure 28 which means that the latent energy of the retentate also has a moderate range between each simulation. The change in cooling required by the evaporator only has a range of 3°F; meaning that each retentate stream has to cool by 6-9°F to reach saturation. Since this is a small range, the specific cooling energy of each retentate stream is nearly the same and the energy savings are not strongly impacted by specific heat. Once the

evaporator has caused saturation, the amount of water that must condense out of the air varies from 0.0156-0.0244 pounds of water per pound of air. The heat of condensation of water is large; large enough to cause huge energy requirements to condense larger amounts of water. The large difference between water content and latent heat in the retentate explains why the relative energy savings in Figure 29 have such a strong dependency on flow rates.

Permeation Coefficient and Selectivity

The permeability or the permeation coefficient of a molecule through a membrane describes a relation between the membrane material and the vapor molecules. Thus, the permeation coefficient will vary for different membranes. The moisture permeabilities of several polymeric materials are shown in Table 6; some are listed by their trade names.

Table 6: Water permeabilities of various polymers reported in units of Barrer[4] (Welding 2013, Metz 2003)

Polymer	Water Permeability (Barrer)	Source
Saran ™	1	Welding 2019
Teflon™	5	Welding 2014
HDPE™	9	Welding 2017
Teflone FEP™	17	Welding 2015
Polypropylene	35	Welding 2018
LDPE™	68	Welding 2016
PVC ™ (unplasticized)	275	Welding 2013
Polyimide	640	Metz 2003
Polystyrene	970	Metz 2004
Lexan ™	1,400	Welding 2021
Natural Rubber	2,600	Metz 2006
Polysulfone	2,620	Metz 2005
Plexiglas™	3,200	Welding 2020
Cellulose acetate	6,000	Metz 2007
Ethyl cellulose	20,000	Metz 2008
PDMS	36,000	MedArray

[4] One Barrer equals 10^{-10}*cm^3(STP)*cm/(cm^2*sec*cmHg).

The comparison in Table 6 shows that permeability data varies from one membrane to another. L.Z. Zhang's study (Zhang 2012) used a liquid composite membrane of cellulose acetate and polyvinylidene fluoride which had an apparent water permeability of about $9x10^6$ Barrer, giving it a higher permeability than any of the other polymers listed in Table 6. Note that since Zhang used a supported liquid membrane, the permeability coefficient should be a description of the solution-diffusion of the vapor through only the liquid layer. However, since Zhang reported mass transfer as NTUm of the entire composite membrane, the conversion from NTUm to Barrer actually gives an apparent permeability, and is not truly descriptive of the permeation of water vapor through the LiCl liquid layer. Even so, liquid membranes have been shown to have a permeability that is 3-4 orders of magnitude higher than that of solid membranes due to differences in diffusion rates (Zhang, Xiao 2008, Pan et al. 1978, Debeaufort et al. 1994, and Isetti 1997).

Figure 30 shows the effect of changing the water permeability while keeping the selectivity constant at 100. This caused a trend of decreasing humidity ratio with increasing water permeability.

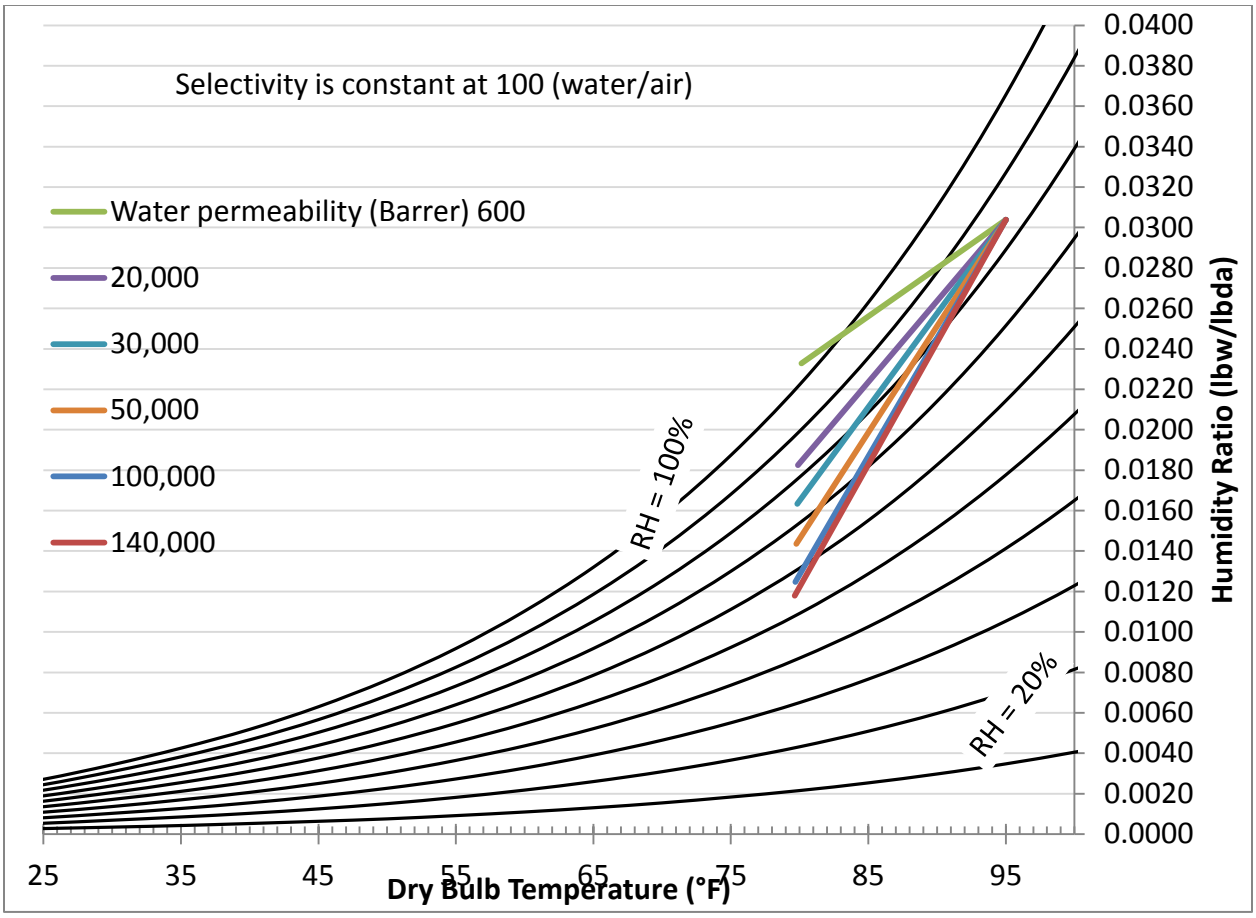

Figure 30: Effect of changing the permeability of water while keeping the permeability of air constant at 600 Barrer. All other parameters are at base levels (see Table 5).

The quality metric of simulations run with water permeabilities equal to or less than 1000 Barrer were less than 70% suggesting that the model was forced past its limitations. Indeed this is shown in Figure 30 by the simulation of 600 Barrer which resulted in the retentate becoming saturated. Similarly, for water permeabilities that were much higher than 200,000, the model was unable to converge within the norms of the model. The permeability of water is directly proportional to the molar flow of water permeating through the membrane. Equation 2 shows this and, once again, it is reprinted below:

$$wa(i) = a \cdot \frac{D_a}{t} \cdot (pf \cdot x(i) - pp \cdot y(i)) \qquad (2)$$

The water molar flow at step "i" is represented by wa(i) which is in direct correlation with D_a, the water permeability coefficient. Increasing the water permeability will increase the

flowof water through the membrane which means that more water vapor permeates from the feed side to the purge side. This mathematical explanation is supported by the results in Figure 30.

The energy trends are shown in Figure 31 below. The trend shows an increase in energy savings with increasing water permeability. It appears as though the energy savings begins to flatten out as the water permeability increases past 100,000 Barrer.

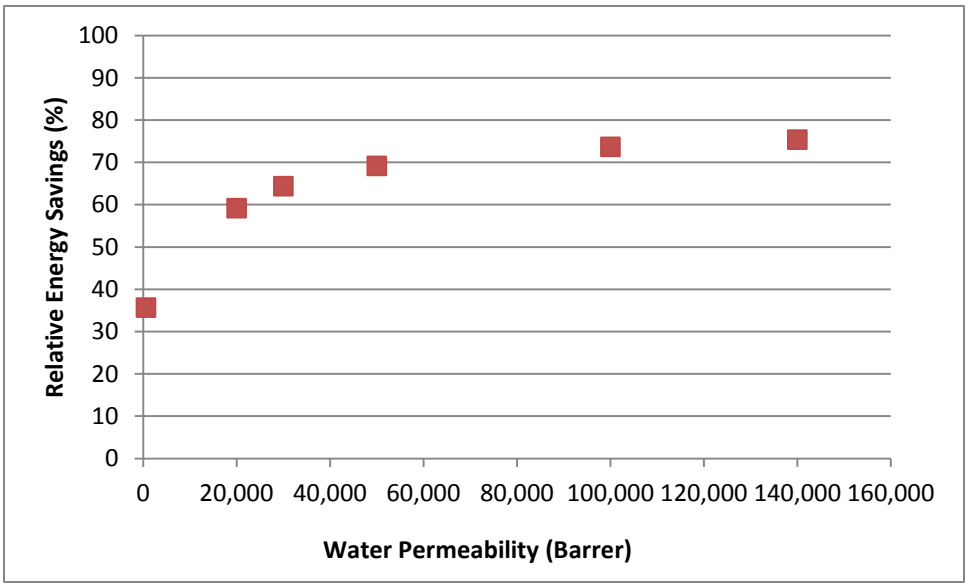

Figure 31: Relative energy savings by varying selectivities by changing the water permeability selectivity constant at 100. All other parameters are at base levels (see Table 5).

Selectivity is the permeability of water divided by the permeability of air. In the above simulations the selectivity was kept constant at a value of 100. This means that as the water permeability increased, so did the air permeability. Since increasing the air permeability increases the air flux into the purge, the air is taken out of the retentate. In other words, increasing the air permeability causes a lower retentate flow rate, and a lower supply of air to the indoor environment i.e. less product. Since the relative energy savings are related to the ratio of delivered air to feed air, a decrease in retentate flow rate will show a decrease in energy savings. This may explain why the energy savings seem to begin to plateau around 100,000 Barrer. Thus it is concluded that the best water permeability will not necessarily be the highest value, because it will depend on the selectivity.

These simulations show that there is some advantage to using a membrane that has high water permeability, such as a supported liquid membrane; however, this advantage may be small. A dense PDMS membrane run at the simulation baseline conditions will have energy savings of 67%, while a liquid membrane of water permeability of 140,000 Barrer will have savings of 75%. This increase of water permeability by nearly 4 times only has an energy savings increase of 8%. But increasing the permeability from 600 Barrer to 100,000 Barrer has an energy savings increase of 38%. This shows that the membrane property of permeability is important to maximize energy savings.

For a case of zero permeability, mass would not be transported across the membrane. Because Kistler and Cussler showed that heat conduction across the membrane is negligible compared to convection due to mass transport, zero permeability would also mean near zero heat transfer in the membrane system. Thus, a hybrid system with no membrane permeability would behave essentially as a traditional DX system.

Figure 32 shows the effect of changing the water permeability from 30,000 to 140,000 Barrer, keeping the permeability of air constant at 400 Barrer. This also means that the selectivity is allowed to vary from 75 to 350. Figure 32 has a trend of increasing water permeability and selectivity decreases the humidity ratio of the retentate.

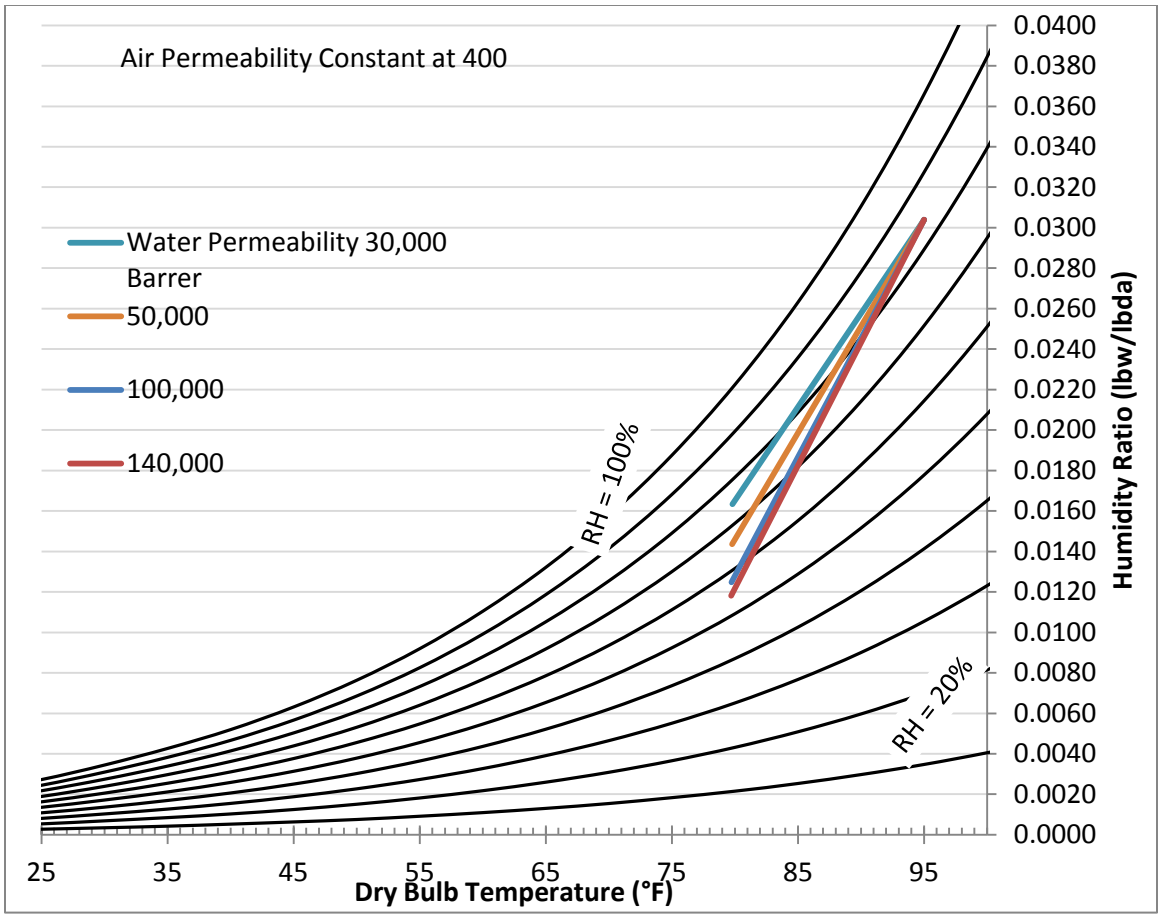

Figure 32: Psychrometric chart of the effect of changing the water permeability and keeping the air permeability constant at 400 Barrer. All other parameters are at base levels (see Table 5).

As with Figure 30, Figure 32 shows that increasing the water permeability and selectivity increases the separation of water by decreasing the humidity ratio of the retentate. This is due to the direct relationship between water permeability and flux as shown in Equation 2 above. The energy analysis of these simulations is shown in Figure 33 for which the trend of energy savings increases with increasing selectivity and increasing water permeability.

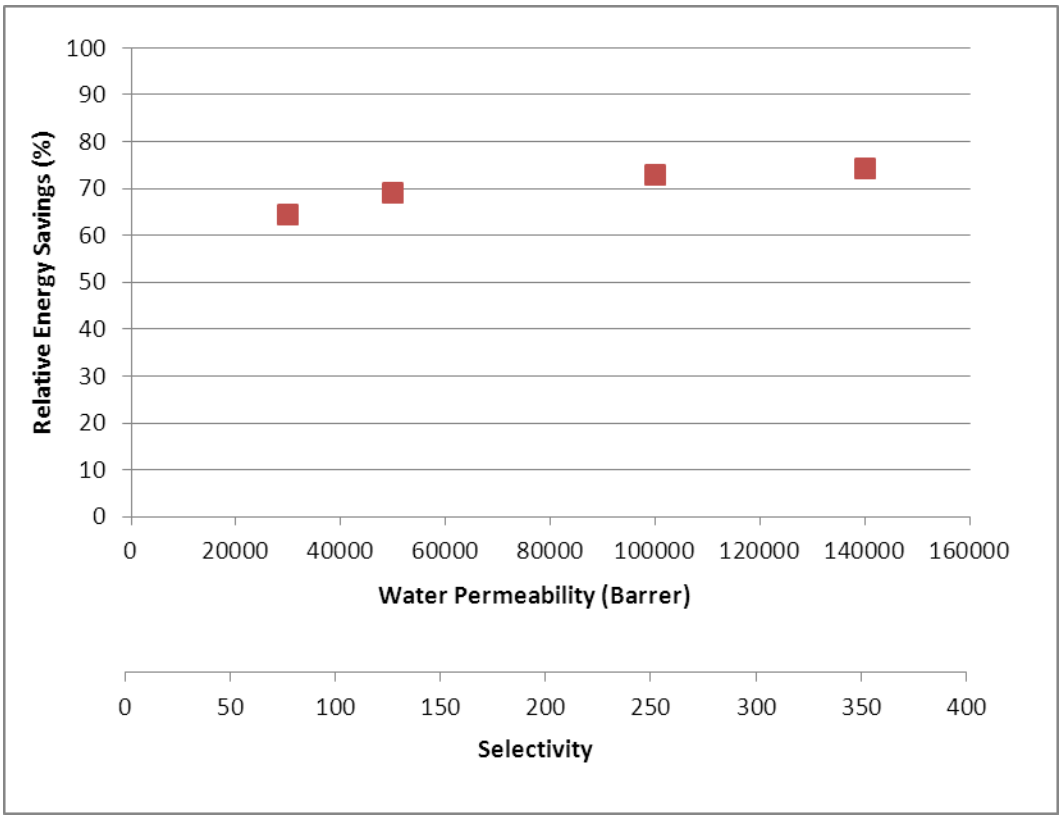

Figure 33: Relative energy savings by varying water permeability, keeping air permeability constant at 400 Barrer. All other parameters are at base levels (see Table 5).

The trend in Figure 33 means that the relative flow rate of air is constant for each retentate stream since the flux of air has not been changed due to constant air permeability. The air permeability is directly related to the molar flow of vapors through the membrane by the following flow equation:

$$w_{air}(i) = a \cdot \frac{D_b}{t} \cdot [pf \cdot (1 - x(i)) - pp \cdot (1 - y(i))]$$

The terms in this equation have been previously discussed in several sections above and their definitions are listed in Table 2. The flow of air through the membrane at step "i", $w_{air}(i)$, is directly proportional to the permeability of air, D_b, in the equation. This relates to the purge flow rate by Equation 5 which has been modified as is shown below:

$$P(i) = P(i + 1) + wa(i) + w_{air}(i) \quad (5)$$

In the above equation, the purge flow rate at location "i+1" increases by the sum of water flow, wa(i), and air flow, $w_{air}(i)$. This means that the purge flow rate at step "i" increases with increasing vapor flux through the membrane. Large increases in the molar flux of air will cause large increases in the purge flow rate. Zero increases in air permeability means zero increases in air flux. Therefore the relative energy savings are unchanged by the air flux. The trends of energy savings are associated only with increases in the water vapor flux which causes decreases in latent energies of the retentate stream. The decrease in latent retentate energy is related to the decrease in water content and corresponding heats of condensation that would otherwise have to be provided by the DX-evaporator. By similar reasoning, one could say that increasing the air permeability would cause energy savings decreases, while increasing water permeability causes increases to energy savings. Therefore the best membrane for an AC system is one that has a high water to air selectivity. Inspection of both Figure 31 and Figure 33 shows that the water permeability and the selectivity have a strong to moderate effect on energy savings.

Cost Estimates

A concern with membrane AC systems is the capital cost of membrane materials and installation. Indeed, some membrane materials may be quite expensive, especially when large areas are required. Table 7 compares several membrane materials. Upon first glance, the material cost of these membranes seems large for such a small area; however, when one square meter of these membranes are added to a DX system that previously operated at $500/year, the payback period for all cases will be less than three years, some less than one year.

Note that comparison between these studies is not entirely equal; this study's simulations has shown that energy savings are impacted by many factors which are not necessarily the same for any two of the studies listed in Table 7 including system type. Furthermore, prices listed in the table are not exact, though they are comparable to each other.

Table 7: This table shows a comparison of costs and benefits of several membrane materials.[5]

Membrane	Price ($/m2)	Source	Maximum Energy Savings	Source	Payback Period (years)
PVDF	590	Sterlitech	50%	Bergero 2010	2.36
PTFE on Polyester	270	Sterlitech	60%	Bergero 2011	0.90
Polysulfone	300	Sterlitech	70%	Kistler 2002	0.86
Composite PVDF and Cellulose acetate	460	Sterlitech	80%	Zhang 2012	1.15
PDMS	490	MedArray	86%	This Study	1.14

In 2002, a study by Kistler and Cussler estimated that a membrane module would cost a maximum of around $75/year/m^2 (Kistler and Cussler, 2002); accounting for 34% inflation (U.S. Inflation 2013) that has occurred in the past decade since Kistler and Cussler's study, their estimate would currently be about $100/m^2. For large membrane systems cost estimates by Bhide and Stern in 1991 were $54/m^2 for material and installation costs (Bhide 1991) inflation would put this estimate currently at $93/m^2 (U.S. Inflation 2013). Current prices of a poly-ethersulfone membrane are at about $200/m^2 (Sterlitech 2013), double of the estimates by previous studies. This suggests that the prices listed in Table 7 are high, though they are within an order of magnitude. This is most likely due to the fact that Sterlitech's products are lab-sized small membranes. The cost of smaller systems is usually much higher than large, bulk products. For MedArray, increasing the size of the PDMS module from 2500cm^2 to 1m^2, an increase 400%, will only increase the price by 167%. Thus, larger modules will be cheaper per unit area than those values listed in Table 7 and will be closer to the estimates of previous studies at around $93-100/m^2. This also means that the calculated payback periods listed in the table are high and it is more likely that the payback period would be less than two years for all membranes shown.

[5] The payback period was calculated by assuming that the old AC system cost $500 per year to operate; and that the membrane installed has an area of 1m^2. These calculations also do not consider cost of installation.

Results Summary

In this chapter the effects of membrane and system properties on the relative energy savings were discussed. The most influential factors impacting energy savings were:

- Flow rate
- Water permeability and selectivity
- Area
- Thickness
- Purge temperature

The flow rate most strongly affects the energy savings. Changing the feed flow rate from 0.002mol/s to 0.008mol/s, while keeping the purge flow constant at 0.002mol/s, had an energy savings decrease of 40%. This is because the purge flow strips water from the feed, less purge flow means a decreased capacity to sweep the flux gas out and away from the feed. Thus a low feed to purge flow ratio is desirable.

The thickness of a membrane depends on its selective layer; results show that energy savings increase with decreasing thickness. Increasing the thickness form 15μm to 120μm decreased the energy savings by 19%. Thus a small thickness is desirable. At extremely low thicknesses mechanical integrity of the membrane will become compromised and so a support structure is required; this type of membrane is called asymmetric.

The purge temperature affects heat exchange in the membrane. Lowering the purge temperature also lowers the retentate temperature; this affects energy savings by bringing the retentate closer to the saturation point, which reduces the cooling load on the evaporator—effectively increasing energy savings. Decreasing the purge temperature by 20°F caused an increase of 24% in the energy savings. Thus a low purge temperature is desirable for high energy savings. Obtaining low purge temperatures will be the source of further discussion.

The permeability and selectivity also have strong effects on the energy savings due to the direct influence of permeability on flux. The results show that energy savings are greater for higher water permeabilities and selectivity. Increasing the water permeability from 600 Barrer to 140,000 Barrer increased the relative energy savings by 39% under constant selectivity. Increasing the selectivity from 75 to 350 increased energy savings by 11%. Thus increasing the

water permeability is desirable, as is increasing the selectivity. However, the benefit of increasing either property becomes less and less with increasing water permeability.

The area had a 30% increase in relative energy savings by increasing the area from 500cm2 to 9500cm2. However, this was not a linear relationship. Increasing the area from 9000 to 9500cm2 only had an increase in energy savings of 1%. Furthermore, increasing the membrane area increases the cost of the membrane since more material would be required. This suggests that the largest membrane area may not be optimal. Calculations would have to be performed for each system to determine the optimal membrane area based on flow requirements, material costs, and separation capabilities.

Of course energy savings can be maximized by combining several of the relationships discussed above. A final simulation was run for which the following properties were used, in Table 8. For convergence to be reached, a single fiber had to be discretized into 200 pieces rather than the usual 100.

Table 8: Input values for a final simulation.

Inputs	
Tf (F)	100
Tp (F)	65
pf (cmHg)	82
pp (cmHg)	74
Da (Barrer)	60,000
Db (Barrer)	347
t (cm)	0.003
F (mol/s)	0.002
P (mol/s)	0.002
L (cm)	8.26
A (cm2)	3500
x(1) (moler)	0.058
y(n) (moler)	0.0115

As shown in Table 8, the inputs in this final simulation were changed to values close to the optimal values of each property to maximize energy savings as discussed. Fans were used to provide pressure. The psychrometric result is shown below in Figure 34.

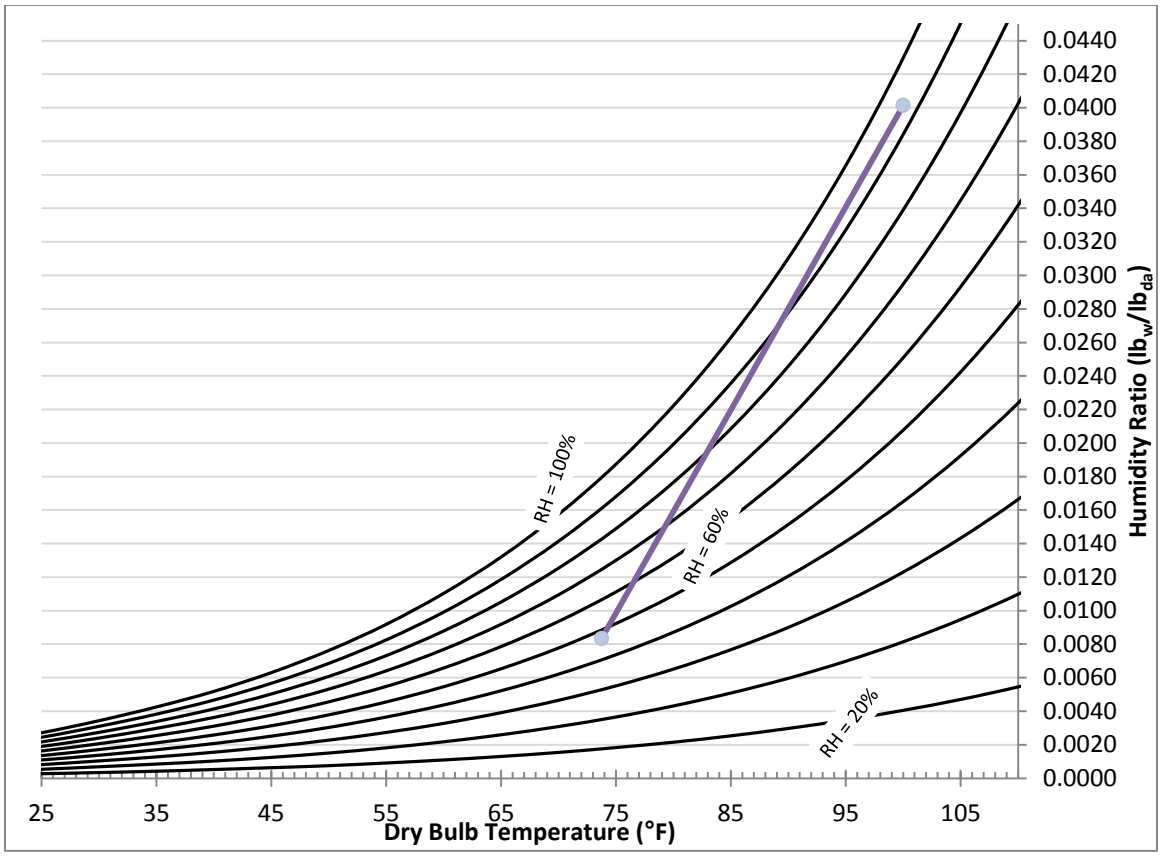

Figure 34: Final simulation for which membrane properties were set at values close to optimal values (in Table 8) for maximizing energy savings.

Figure 34 shows the highest separation of water vapor from an air stream yet seen in any previous simulation. The feed, which was at 100°F and 95% humidity, was treated by the membrane to a retentate of 73°F and 50% relative humidity. In fact, these retentate conditions are cold and dry enough to be supplied indoors without any further cooling or dehumidification. If this was the case, energy savings would be on the order of 95%, since the only electrical requirements would be due to the feed and purge fans. However, if the system does utilize an evaporator and condenser to dehumidify the retentate to 40% humidity and 68°F, then the relative energy savings would be 86%.

This last simulation was reported to illustrate how the combination of membrane properties can have an increased effect on energy savings. Energy savings shown in this final simulation are higher than in any of the other simulations where only one property was influenced at a time. Thus membrane properties do have effects on energy savings.

Chapter 4 - Conclusions and Outlook

Membranes used in air conditioning systems have the potential to decrease energy requirements for treatment of air. These systems have been researched in growing detail for the past 20 years for which 8-80% were found to be possible. However, many of these studies lack details about the behavior of the membrane and the influence its properties have on the overall energy savings. In order to investigate the effects of membrane properties on the energy use of a total membrane heat exchanger (system diagram shown in Figure 4), a model was created and validated. Then membrane properties were varied and simulations were run to investigate their effect on calculated energy savings.

Based on the simulations that were conducted, it was found that there are a lot of factors involved in the performance of a membrane, the most influential were: flow rates, purge temperature, membrane area and thickness, water permeability, and selectivity. The trends presented have shown that high purge flow rates are desired, low purge temperatures, a moderate area, small membrane thickness, high to moderate water permeabilities, and high selectivities. Not all property behavior is linearly related to energy savings. Water permeability and area both begin to plateau with increasing values, suggesting that the optimal water permeability and membrane area is not the highest, but some moderate value. Even if the exact values of the predications are not accurate, the trends in behavior are and choices regarding operation of these membrane systems can be made accordingly.

There are many different types of membranes that can be chosen among for use in a membrane hybrid DX system. Nasif et al. used a porous membrane, which has a low selectivity and moderate permeability coefficient, and had energy savings of 8% (Nasif 2010). Zhang et al. used a supported liquid membrane, which has a high thickness but a large permeability and selectivity, which showed energy savings of up to 80% (Zhang 2012). In the simulations presented here, a dense film was used of moderate thickness and selectivity, with a high permeability and showed energy savings of 86%. These comparisons show that no single membrane system parameter is responsible for maximum energy savings, but energy savings are dependent upon many membrane parameters.

Some implicated challenges of using a membrane based total heat exchanger is for cases in which the feed and purge conditions do not have large differences in temperature or humidity

levels. However, this challenge may be combatted by controlling the pressure. As was shown, a high pressure difference between the feed and purge side causes a larger difference in their partial pressures. Since permeation of gases is driven by the partial pressure difference, separation could be maximized for a variety of feed conditions without much loss in energy efficiency. However, such pressure control may be limited to smaller sized applications such as small domestic AC units or in vehicles which do not require large pressure differences or flow rates, since these rates would be limited to use by a fan.

In addition to controlling the membrane system's performance with pressure, the purge conditions of the hybrid system could be controlled by diverting some of the cold air from the evaporator and mixing it with the purge to create a colder stream for exchange with the feed. This mixing of air would provide another mechanism to control and maximize membrane performance under many different outdoor air conditions.

Of course there are other considerations than energy savings and payback period that should be considered when choosing a membrane. Membrane lifetime and the membrane's chemical resistance to volatile gases and pollutants will impact the actual energy savings and should therefore be considered. Also, temperature resistance may be an issue when using a compressor for which an increase in pressure causes a significant temperature increase.

Other concerns may involve bacterial growth inside the membrane module, which will be related to maintenance and membrane lifespan. Since the inside of the module will be hot and humid for a period of several weeks, at least, bacteria and mold might be able to grow and cause inhibition of the membrane performance by decreasing the available membrane area. This is another concern which will have to be addressed for application of the membrane hybrid DX system.

Future work on the topic of membrane hybrid DX systems should include experimental validation of the above model. Different membrane materials may influence the validity of the model's assumptions. Experimental evidence may show a dependence of permeability on temperature or significant thermal conductivity of the membrane material; these effects would negate the validity of the model and the assumptions stated in Chapter2.

Future work of hybrid systems should also include a sensitivity analysis and optimization of multiple variables simultaneously. Also, comparison of the energy performances of the hybrid

system to other types of AC processes (other than the simplistic traditional DX system) could prove useful for eventual implementation of the hybrid system.

The advantages of using a membrane total heat exchanger include its simplicity with no moving parts, its compactness, and its compatibility with currently existing processes. The membrane materials mentioned here are commonly used and readily available. These membrane DX systems have been studied for the past 20 years and have consistently shown substantial energy savings. Simulations have shown results as high as 86-95% energy savings. These savings could contribute to reducing global AC energy use by more than half.

References

Baker, R.W., *Membrane Technology and Applications*, McGraw-Hill, 2000.

Bergero, S., A. Chiari, On the performances of a hybrid air-conditioning system in different climatic conditions, Energy, Vol 36, July 2011.

Bergero, S., A. Chiari, Performance analysis of a liquid desiccant and membrane contactor hybrid air-conditioning system, Energy and Buildings, Vol 42, June 2010.

Bhide, B.O., Stern, S.A., A New Evaluation of Membrane Processes for the Oxygen enrichment of Air, Journal of Membrane Science, Vol. 62, 1991, p. 87.

Bureau of Energy Efficiency, Fans and Blowers, Chapter 5, http://www.saylor.org/site/wp-content/uploads/2011/09/Chapter-3.5-Fans-Blowers.pdf, April 3, 2013.

Chiou et al., The study of energy-saving strategry for direct expansion air conditioning system, Energy and Buildings, Vol 40, Feb 2008.

Costello, L.M., W.J. Koros, *Effect of Structure on the Temperature Dependence of Gas Transport and Sorption in a Series of Polycarbonates*, Journal of Polymer Science, 32, 1994.

Cox, Stan. "Cooling a Warming Planet: A Global Air Conditioning Surge", Yale E360, July 2012.

Debeaufort, Voilley, Meares, Water vapor permeability and diffusivity through methylcellulose edible films, J. Membrane Science, Vol 91, 1994.

EIA. U.S. Energy Information Administration, http://www.eia.gov/tools/faqs/faq.cfm?id=23&t=10, April 11, 2013.

Hemingson. et al., Steady-State performance of a run-around membrane energy exchanger (RAMEE) for a range of outdoor air conditions, International Journal of Heat and Mass Transfer, Vol 54, Feb. 2011.

Image, May 5, 2013 < http://www.gewater.com/handbook/ext_treatment/fig9-5.jsp.>.

Incropera, DeWitt, Bergman, Lavine, *Fundamentals of Heat and Mass Transfer*, 6th Edition, John Wiley & Sons, 2007.

Isetti et al., On the application of a membrane air-liquid contactor for air dehumidification, Energy and Buildings, Vol 25, 1997.

Johnson et al., Analysis of heat and mass transfer phenomena in hollow fiber membranes used for evaporative cooling, Journal of Membrane Science, Vol 227, August 2003.

Kistler, K.R., E.L. Cussler, Membrane modules for building ventilation, Trans IChemE, Vol 80, Jan. 2002.

Koros, W.J. D.G. Woods, *Elevated temperature application of polymer hollow-fiber membranes*, Journal of Membrane Science, 181, 2001.

Kozubal et al., Desiccant enhanced evaporative air-conditioning (DEVap): Evaluation of a new concept in ultra efficient air conditioning, NREL technical report, Jan 2011.

Liang et al., Performance analysis of a direct expansion air dehumidification system combined with membrane-based total heat recovery, Energy, Vol 25, June 2010.

Mahmud et al., Performance testing of a counter-cross-flow run-around membrane energy exchanger (RAMEE) system for HVAC applications, Energy and Buildings, Vol 42, Feb 2010.

MedArray, Inc., http://permselect.com/membranes/, November 1, 2012.

Metz, S.J., *Water Vapor and Gas Transport through Polymeric Membranes*, PhD Thesis, University Twente, 2003.

Nasif et al., Membrane heat exchanger in HVAC energy recovery systems, systems energy analysis, Energy and Buildings, Vol 42, May 2010.

Pan, Jensen, Pielech, Habgood, Permeation of water vapor through cellulose triacetate membrane in hollow fiber form, J. Applied Polymer Science, Vol 22, 1987.

Sterlitech Corporation, http://www.sterlitech.com/membrane-disc-filters.html, April 3, 2013.

U.S. Inflation Calculator, http://www.usinflationcalculator.com/, April 15, 2013.

University of Illinois, Mechanical Engineering PowerPoint, *Isentropic Efficiencies of Turbines Compressors, and Nozzles*, November 3, 2008.

Welding Journal, http://www.faybutler.com/pdf_files/HowHoseMaterialsAffectGas3.pdf, April 16, 2013.

Wind, Staudt-Bickel, Paul, Koros, Effects of Crosslinking chemistry on CO2 Plasticization of Amide Gas Separation Membranes, Ind. Eng. Che. Res., Vol 41, 2002.

Zhang, L.Z., Progress on heat and moisture recovery with membranes: From fundamentals to engineering applications, Energy Conversion and Management, 63, 2012.

Zhang, Xiao, Simultaneous heat and moisture transfer through a composite supported liquid membrane, International Journal of Heat and Mass Transfer, 51, 2008.

Zhang, Zhang, Miao, Pei, Selective permeation of moisture and VOCs through polymer membranes used in total heat exchangers for indoor air ventilation, Indoor Air, Vol 22, 2011.

Appendix A - Matlab Model Code

```
%Model by Liz Boyer
%membrane dehumidification of air

Tf=95; %Temperature of the outside air in Fahrenheit
Tf=(Tf-32)*5/9+273; %in kelvin

Tp=75; %temperature of the purge indoor air going into the membrane in
Farenheit
Tp=(Tp-32)*5/9+273; %in kelvin

pf=80; % Feed side pressure (cmHg)
pp=76; % Permeate side pressure (cmHg)

Da=36000*10^-10; %A permeability (Barrer*10^-10)
Db=347*10^-10; %B permeability (Barrer*10^-10)

t=55*10^-4; %membrane thickness (cm)

F=.002; %Feed entry flow rate (mol/s)
Fo=F*22414; %Feed flow rate (cm3(STP)/s)

P=.002; %Permeate entry flow rate (mol/s)
Po=P*22414; %Permeate entry flow rate (cm3(STP)/s)

n=100; %total number of small balance boxes

L=8.26; %cm length of tube
Diam=190*10^-3;  % inner diameter of the fibers (cm)

A=2500; %total membrane surface area (cm2)
a=A/n; %surface area of small balance box

x(1)=.043898; %feed entering mol fraction of 84% relative humidity

y(n)=.0161; %permeate entering mol fraction of 40% RH

%%%%%%%%%%%%%%%%%%%%%%%%%%%%%%%%%%%%%%%%%%%%%%%%%%%%%%%%%%%%%%%%%%%%%%%%%%%
cp=1.007; %specific heat capacity of air at 300K (in J/g/K) same for both
sides assume constant
visc=15*10^-6; %in (m2/s)
kair=26*10^-3; %(W/m/K) assume is constant
dens=1.16; %(kg/m3) density of air assume constant
Pr=cp*1000*dens*visc/kair; %from Appendix A of Incropera & DeWitt 2007 at
300K

if pf>84
    Thot=Tf*(pf/76)^0.318; %Using a compressor 0.318=R/cp, R is universal gas
constant for air.
else
    Thot=Tf;
```

```
end
Tcold=Tp;

%Guesses
Ye=y(n)*3; %exhaust mol frac A in Permeate must be higher than ya(n)
E=P*3; %exhaust flow rate from permeate side (mol/s)
Te=(90-32)*5/9+273;

E=E*22414; %(cm3(STP)/s)
yo=y(n);
s=(Ye-yo)/(n); g=(E-Po)/(n); b=(Te-Tp)/n;i=1;
while i<n %creating initial guesses for permeate side fractions and flows
    Ya(i)=Ye-s*(i-1);
    P(i)=E-g*(i-1);
    Tc(i)=Te-b*(i);
    Tco(i)=Te-b*(i-1);
    i=i+1;
end
Tco(1)=Te;

Ya(n)=y(n);P(n)=Po; Tc(n)=Tcold; Th(1)=Thot;
i=1;
k=1;
F(1)=Fo;
E(1)=E;
Pcum=Po; W(n)=0; %at n entry permeate

while k<500 %mass transfer and heat transfer calculations
    while i<n
        y(i)=(Da/t*(pf*x(i)-pp*Ya(i))+P(i)*Ya(i))/(Da/t*(pf*x(i)-
pp*Ya(i))+P(i)+Db/t*(pf*(1-x(i))-pp*(1-Ya(i))));
        wa(i)=a*Da/t*(pf*x(i)-pp*y(i));
        W(i)=wa(i)+a*Db/t*(pf*(1-x(i))-pp*(1-y(i)));
        R(i)=F(i)-W(i);
        x(i+1)=(x(i)*F(i)-wa(i))/R(i);
        F(i+1)=R(i);
        i=i+1;
    end
    i=n-1;
    while i>0 %letting i=1 permeate exaust be determined by mass balance.
Walking backwards relative to feed flow.
        P(i)=P(i+1)+W(i);
        Ya(i)=(y(i+1)*P(i+1)+wa(i))/P(i); %new guess values that are closer
to calculations
        i=i-1; %working backwards. Forwards on the permeate side
    end
    i=1;
    while i<n
 %assume external flow
        Relh=F(i)*4*L/(visc*100^2)/Diam^2/pi;
        Relc=P(i)*4*L/(visc*100^2)/Diam^2/pi;
        if Relh<5000
            Nuh=0.664*Relh^(1/2)*Pr^(1/3); %Nu and Re correlations from table
7.9 in Incropera & DeWitt 2007
        else
            Nuh=0.0296*Relh^(4/5)*Pr^(1/3);
```

```
        end
        if Relc<5000
            Nuc=0.664*Relc^(1/2)*Pr^(1/3);
        else
            Nuc=0.0296*Relc^(4/5)*Pr^(1/3);
        end
        hh=Nuh*kair/(L/100); % (W/m2/K)
        hc=Nuc*kair/(L/100);

        U(i)=(abs((1/hh)+(1/hc))^-1)/100^2; %in W/cm2K
        if F(i)>P(i)
            Cmin(i)=P(i)*cp/22414*(18*y(i)+26*(1-y(i))); %converting flow to
g/s so Cmin is (g/s*J/g/K)
            Cr(i)=P(i)/F(i);
        else
            Cmin(i)=F(i)*cp/22414*(18*x(i)+26*(1-x(i)));
            Cr(i)=F(i)/P(i);
        end
        NTU(i)=U(i)*a/Cmin(i)/100^2;
        qmax(i)=Cmin(i)*(Th(i)-Tc(n+1-i));
        ee(i)=(1-exp(-NTU(i)*(1-Cr(i))))/(1-Cr(i)*exp(-NTU(i)*(1-Cr(i))));
%assumes heat exchange is a concentric tube, counterflow with Cr<1
        q(i)=ee(i)*qmax(i);
        Tho(i)=Th(i)-(q(i)/(F(i)*cp/22414*(18*x(i)+26*(1-x(i)))));
        Th(i+1)=Tho(i);
        i=i+1;
    end
    i=1;
    q(n)=q(99);
    while i<n
        Tco(n+1-i)=Tc(n+1-i)+(q(n+1-i)/(P(n+1-i)*cp/22414*(18*y(n+1-i)+26*(1-
y(n+1-i)))));
        Tc(n-i)=Tco(n+1-i);
        i=i+1;
    end
    Te=Tco(1);
    i=1; b=(Te-Tp)/n;
    while i<n %re-evaluating cold side profile
        Tc(i)=Te-b*(i);
        Tco(i)=Te-b*(i-1);
        i=i+1;
    end
    i=1;
    while i<n %evaluating hot side profile
        Tho(i)=P(i)/F(i)*-(Tco(i)-Tc(i))+Th(i);
        Th(i+1)=Tho(i);
        Tco(i+1)=Tc(i);
        i=i+1;
    end
    i=n-1;
    i=1;
    k=k+1;

end

%calculating overall transfer units
```

```
qmax= Cmin(n/2)*(Th(1)-Tc(n));
q=P(n/2)*cp/22414*(18*y(n/2)+26*(1-y(n/2)))*(Th(n/2)-Tc(n/2));
ee=q/qmax;
NTU=(1/(Cr(n/2)-1))*log((ee-1)/(ee*Cr(n/2)-1)); %counterflow concentric tube
table 11.4 Incropera
%high NTU means higher transfer which is good
NTUm=(A/100^2)/(F(1)/22414/1000*26*18/26*(x(1))/(1-
x(1)))*(100/t)*Da*(pf*x(1)-pp*y(n))/22414*18*100/1000; %used water flow
because we used the water permeability

i=1;
wa(n)=0;
while i<n+1
    I(i)=i;
    i=i+1;
end

Ppa=(y)*pp;
Pfa=(x)*pf;

S=5;
figure;
subplot(1,2,1)
scatter(I,Ppa,S,[0 1 0]) %green permeate partial pressure (cmHg)
hold on
scatter(I,Pfa,S,[0 0 0]) %black feed partial pressure (cmHg)

subplot(1,2,2)
scatter(I,Th,S,[1 0 0]) %red feed temperature (Kelvin)
hold on
scatter(I,Tc,S,[0 1 1]) %cyan permeate temperature(Kelvin)

xenter=x(1);
xexit=x(n);
yenter=y(n);
yexit=y(1);
Te=(Tc(1)-273)*9/5+32;
Tr=(Th(n-1)-273)*9/5+32;
NTU;
NTUm;
selectivity=Da/Db;
sep_ratio=(x(1)-x(n))/x(1);
Ff=F(1);
Rr=R(n-1);
Daw=Da*10^10;
Thot=(Thot-273)*9/5+32;
Tcold=(Tcold-273)*9/5+32;
Data={Daw,selectivity,pf,pp,A,t,NTU,ee,NTUm,L,Thot,Tcold};

filename='results1.xlsx';
sheet=1;
xlswrite(filename,I,sheet,'1');
xlswrite(filename,x,sheet,'2');
xlswrite(filename,y,sheet,'3');
xlswrite(filename,Th,sheet,'4');
xlswrite(filename,Tc,sheet,'5');
```

```
xlswrite(filename,F,sheet,'6');
xlswrite(filename,P,sheet,'7');
xlswrite(filename,Data,sheet,'8');
```